論文 / 著書情報
Article / Book Information

題目(和文)	CLIP-170は細胞接着面におけるダイニン配置を制御することにより T細胞活性化における中心体の細胞接着面近傍への移動に必須の役割を果たしている
Title(English)	CLIP-170 is essential for MTOC repositioning during T cell activation by regulating dynein localisation on the cell surface
著者(和文)	LimWei Ming
Author(English)	Wei Ming Lim
出典(和文)	学位:博士(工学), 学位授与機関:東京工業大学, 報告番号:甲第11101号, 授与年月日:2019年3月26日, 学位の種別:課程博士, 審査員:德永 万喜洋,粂 昭苑,山口 雄輝,川上 厚志,立花 和則
Citation(English)	Degree:Doctor (Engineering), Conferring organization: Tokyo Institute of Technology, Report number:甲第11101号, Conferred date:2019/3/26, Degree Type:Course doctor, Examiner:,,,,
学位種別(和文)	博士論文
Type(English)	Doctoral Thesis

CLIP-170 is essential for MTOC repositioning during T cell activation by regulating dynein localisation on the cell surface

Department of Biological Information
School of Life Science and Technology
Tokyo Institute of Technology

March 2019

LIM WEI MING

Academic Supervisors Prof. Makio Tokunaga
Assoc. Prof. Kumiko Sakata-Sogawa

Table of content

List of Figures

Chapter 3 figures

List of tables

Nomenclature

AMPK	:	adenosine monophosphate-activated protein kinase
APC	:	antigen presenting cell
A.U.	:	arbitrary unit
CAP-Gly	:	cytoskeletal-associated protein glycine-rich domain
cDNA	:	complementary deoxyribonucleic acid
CLIP-170	:	cytoplasmic linker protein 170
cSMAC	:	central supramolecular activation cluster
DLC	:	dynein light chain
DMSO	:	dimethyl sulfoxide
EB1	:	end-binding protein 1
GDP	:	guanosine diphosphate
GTP	:	guanosine triphosphate
CLIP-170	:	cytoplasmic linker protein 170
IS	:	immunological synapse
LFM	:	low fluorescence medium
MHC	:	major histocompatibility complex
MT	:	microtubule
MTOC	:	microtubule-organizing center
PBS	:	phosphate buffered saline
ROI	:	region of interest
SDM	:	site directed mutagenesis
shRNA	:	small hairpin ribose nucleic acid
TCR-MCs	:	T cell receptor microclusters
TIR	:	total internal reflection

Abstract

The microtubule-organizing centre (MTOC) is repositioned to the centre of the contacted cell surface, the immunological synapse, during T cell activation. However, our understanding of its molecular mechanism remains limited. Here, we found that the microtubule plus-end tracking cytoplasmic linker protein 170 (CLIP-170) plays a novel role in MTOC repositioning using fluorescence imaging. Inhibition of CLIP-170 phosphorylation impaired both MTOC repositioning and interleukin-2 (IL-2) expression. T cell stimulation induced some fraction of dynein to colocalise with CLIP-170 and undergo plus-end tracking. Concurrently, it increased dynein in minus-end-directed movement. It also increased dynein relocation to the centre of the contact surface. Dynein not colocalised with CLIP-170 showed both an immobile state and minus-end-directed movement at a velocity in good agreement with the velocity of MTOC repositioning, which suggests that dynein at the immunological synapse may pull the microtubules and the MTOC. Although CLIP-170 is phosphorylated by AMP-activated protein kinase (AMPK) irrespective of stimulation, phosphorylated CLIP-170 is essential for dynein recruitment to plus-end tracking and for dynein relocation. This indicates that dynein relocation results from coexistence of plus-end- and minus-end-directed translocation. In conclusion, CLIP-170 plays an indispensable role in MTOC repositioning and full activation of T cells by regulating dynein localisation.

Chapter 1

General Introduction

T cell activation is an essential step of the immune response. It is initiated by the recognition of the specific antigen displayed on the surface of an antigen-presenting cell (APC). The T cell receptor (TCR)/CD3 complex, composed of TCR subunits and CD3 subunits, recognizes antigenic peptides presented by major histocompatibility complex (MHC) molecules. This activation triggers the immune response in T cells, including cytokine production such as interleukin 2 (IL-2), and the dynamic reorganization of signalling molecules, as well as reorganization of actin and microtubule cytoskeletons. At the interface between the T cell and the APC, TCR signalling and related molecules are reorganized to the immunological synapse[1,2], where the initial stages of the signaling cascade are spatiotemporally controlled on TCR/CD3 microclusters[3]. At almost the same time, MTOC undergoes dynamic repositioning and is moved to the immunological synapse[4–9] (Fig. 1.1), where secretory vesicles are accumulated to allow focused secretion against the target cell[10,11].

As for the driving motive force of MTOC movements, several lines of evidence have shown the involvement of cytoplasmic dynein, the major microtubule minus-end-directed motor protein, in MTOC repositioning[6–9,12,13]. Imaging of microtubules showed that the MTOC was pulled by microtubules, suggesting that dynein drives MTOC repositioning in T cells[6–9]. Depletion of dynein using small interfering RNA (siRNA) or inhibition of dynein activity with ciliobrevin was shown to prevent MTOC repositioning[7,9].

Cytoplasmic dynein is involved in a variety of cellular functions, and its motor activity is regulated spatiotemporally by its interaction with a variety of regulatory proteins[14–16]. Dynein is a 1.4 MDa protein consisting of two copies of six different subunits, and this elaborate structure enables dynein to have a variety of activity. Recent studies with recombinant human dynein have unravelled the mechanism underlying its multimodal motor activities:

auto-inhibited (dynein alone), weakly processive (dynein alone) and highly processive (dynein/dynactin/cargo-specific adaptor protein complex) using single-molecule techniques[17–21], X-ray crystallography[22] and cryo-electron microscopy (Fig. 1.2)[23].

Given that dynein is anchored at the immunological synapse, its processive activity could pull on the microtubules. A candidate for the anchor is a dynein-binding protein, nuclear distribution E homolog 1 (NDE1), which functions to associate dynein with membranes[24]. NDE1 accumulates at the immunological synapse, whereas NDE-like 1 (NDEL1), a NDE1 homologue, does not[25]. Furthermore, knockdown of NDE1 in T cells were shown to inhibit MTOC translocation[25].

Two mechanisms for targeting dynein to the plus end are known[26]. First, a subset of plus-end tracking proteins (+TIPs), such as +TIP end-binding protein EB1, CLIP-170 and dynactin, recruits dynein the plus-end[27,28]. Second, kinesin motor proteins complexed with CLIP-170 transport dynein-Lis1 complexes along microtubules to the plus end, and EB1 mediates loading of kinesin-CLIP-170 complexes onto microtubules[29,30].

CLIP-170[31,32], the key molecule in targeting dynein to the plus end, binds microtubules via EB1[33]. CLIP-170 contains two N-terminal CAP-Gly (cytoskeleton-associated protein glycine-rich) domains acting as the binding site for EB1, a central long coiled-coil dimerization domain, followed by tandem C-terminal Zn^{2+} knuckle domains, and an ETF motif[34]. Dynactin and Lis1 competitively bind to the C-terminal domains of CLIP-170[35]. CLIP-170 is also responsible for the regulation of microtubule dynamics. CLIP-170 phosphorylated by AMP-activated protein kinase (AMPK) rapidly dissociates from the microtubule and promotes efficient microtubule polymerization (Fig. 1.3)[36]. As depletion of CLIP-170 was reported to block MTOC repositioning and to function at the cell periphery in B cells[12], CLIP-170 is likely responsible for MTOC repositioning during B cell activation. However, the role of CLIP-170 on MTOC repositioning and how dynein is translocated to the immunological synapse in T cells have not been uncovered.

In this study, the role of CLIP-170 in MTOC repositioning and its interaction with dynein involved in this process during T cell activation were investigated. First, in chapter 2, using fluorescence microscopy, MTOC repositioning was dissected into two directions; parallel and perpendicular to the contact surface. CLIP-170 and its phosphorylation were shown to be critical for MTOC centering. Then, in chapter 3, using simultaneous dual-colour fluorescence imaging of CLIP-170, dynein and/or dynactin, their colocalisation and motility states were examined. Dynein relocation to the immunological synapse was discovered to rely on the coexistence of plus-end- and minus-end-directed translocation due to CLIP-170 and T cell stimulation.

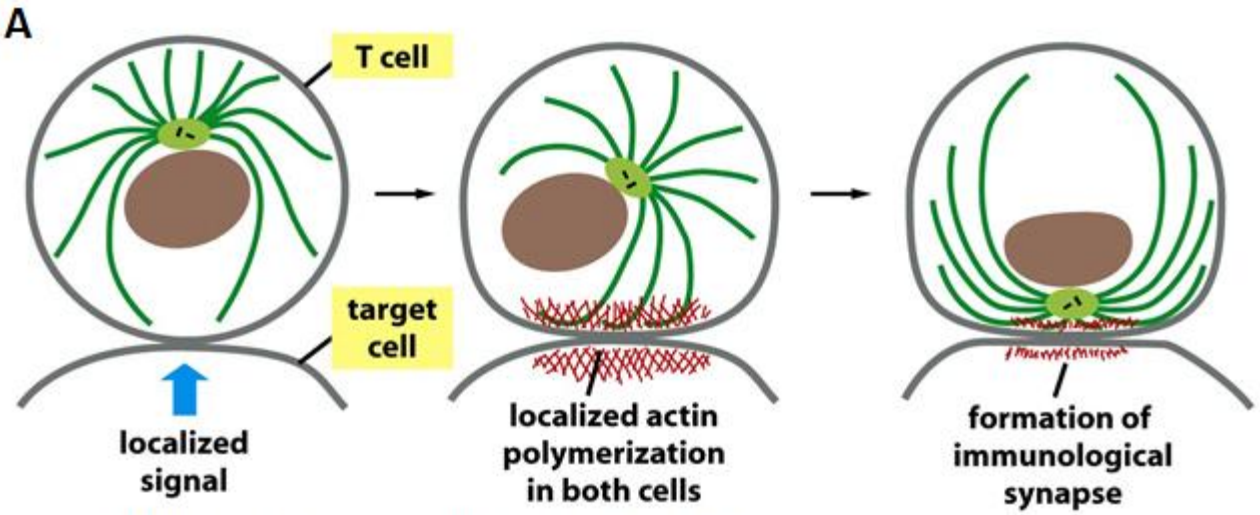

Figure 16-103a Molecular Biology of the Cell 5/e(©Garland Science 2008)

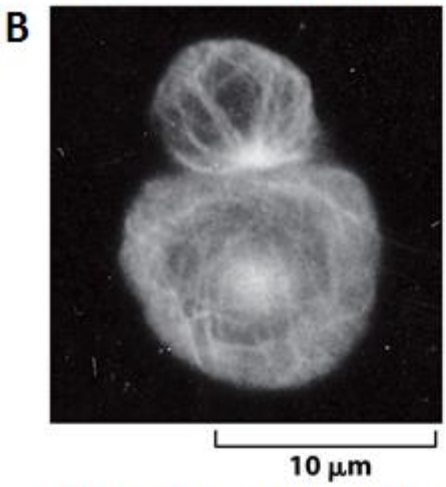

Figure 16-103b Molecular Biology of the Cell 5/e(©Garland Science 2008)

Figure 1.1 MTOC repositioning during T cell activation. (**A**) A model of MTOC repositioning upon T cell stimulation. (**B**) Indirect immunofluorescence labeling for tubulin of CTL-TC conjugates to show the MTOC of the CTL (smaller cell) and the TC (larger cell), respectively[4].

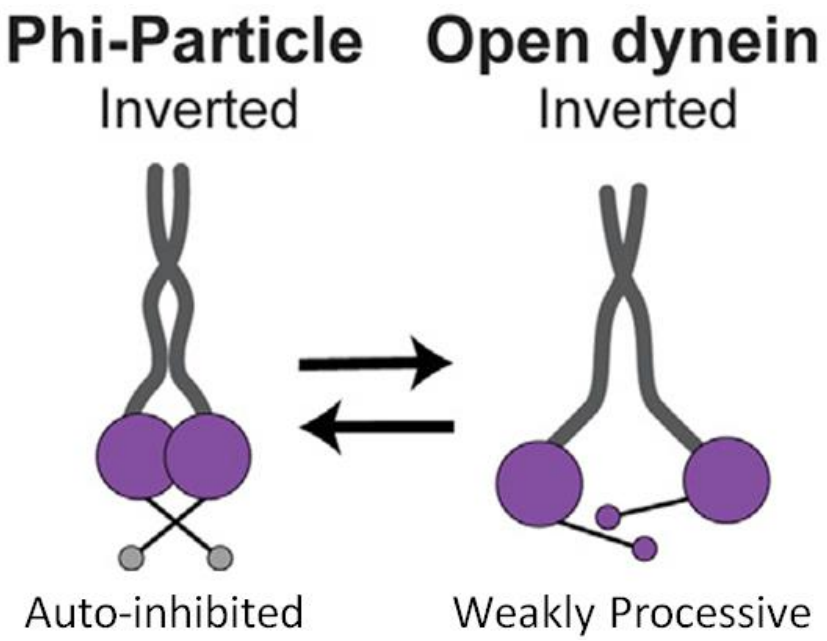

Figure 1.2 A model describing the dynein forms[23]. Isolated dynein exists in either the phi-particle (motors dimerized, low affinity for the microtubule) or the open form (increased microtubule affinity).

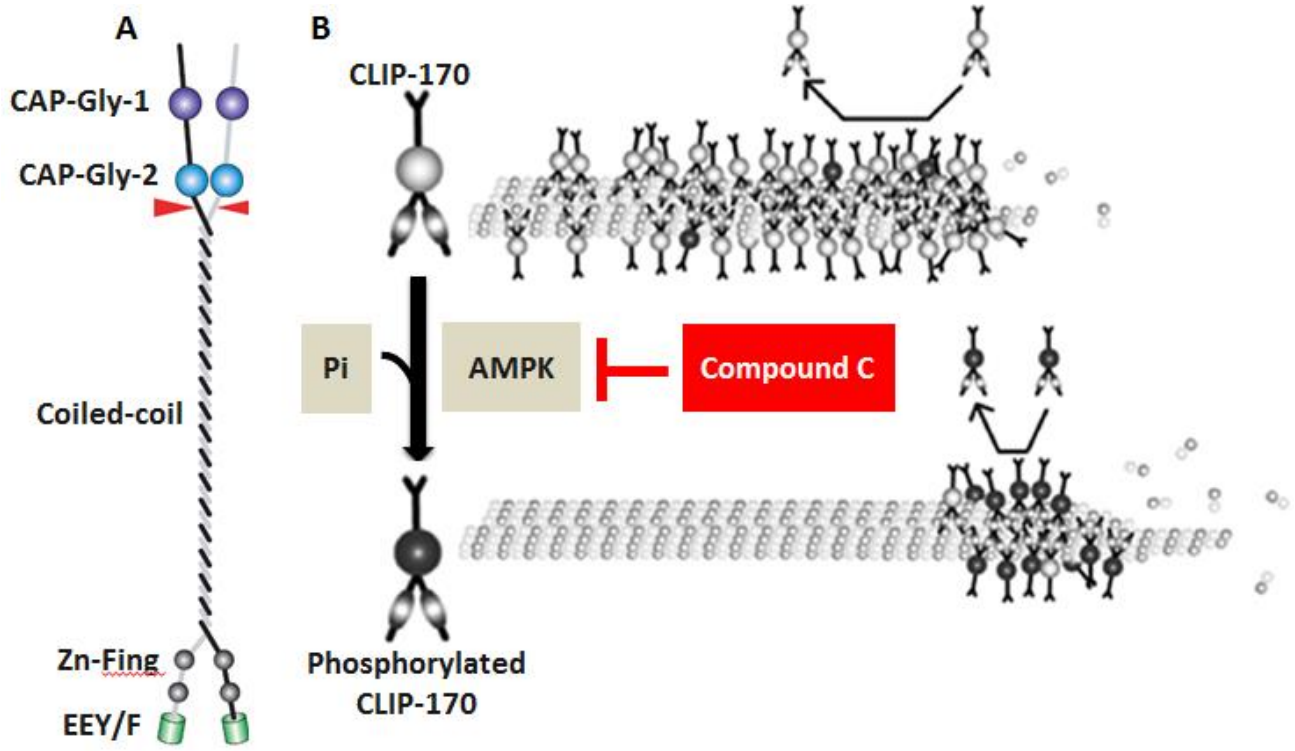

Figure 1.3 CLIP-170 structural model and its interaction with adenosine monophosphate-activated kinase (AMPK) in regulating efficient microtubule polymerization[36]. (**A**) Structural model of CLIP-170. Ser-312 indicated by red is located between the CAP-Gly-2 domain and the coil-coil region in CLIP-170. CAP-Gly, cytoskeleton associated protein Glycine-rich; Zn-Fing, C-terminal zinc knuckle of CLIP-170; EEY/F, C-terminal amino sequence of CLIP-170. (**B**) AMPK phosphorylates CLIP-170 at its coiled-coil region. The phosphorylation of CLIP-170 by AMPK is required for the efficient polymerization of microtubules. Phosphorylated CLIP-170 rapidly detaches from the microtubule lattice, contributing to efficient microtubule polymerization. In contrast, the inhibition of AMPK results in the prolonged and enhanced accumulation of nonphosphorylated CLIP-170 on the microtubule lattice, leading to the disturbance of microtubule polymerization.

Chapter 2

CLIP-170 regulates MTOC repositioning and full T cell activation

2.1 Introduction

CLIP-170, a microtubule plus-end binding protein binds and dissociates rapidly from the growing microtubule plus-end through phosphorylation mediated by AMPK[33,36]. In succession, this regulates the microtubule plus-end dynamics. AMPK, apart from mediating CLIP-170 phosphorylation at Ser-312, it also functions to regulate T cell activation and immune responses, indicated by the increase expression of IL-2, a cytokine signaling molecule[40]. In good agreement, recent study shows CLIP-170 knockdown in B cell impairs MTOC relocation[12], suggesting CLIP-170 crucial role in mediating MTOC repositioning. However, in T cell, it remains unclear the role of CLIP-170 phosphorylation on MTOC repositioning.

In this chapter, the role of CLIP-170 on MTOC repositioning was examined using fluorescence microscopy. Fluorescence microscopy is a simple yet powerful tool for investigating cellular activities. Total internal reflection fluorescence microscopy (TIRFM) can capture images of surface-bound proteins by selectively excites only the surface-bound fluorophores, while the non-bound ones are left unexcited. Switching from TIRFM to epi-illumination allows quantitative measurement of protein distance from cell surface, making this technique a compelling tool for MTOC repositioning study.

Using fluorescence microscopy equipped with TIRF and epi-illumination, MTOC repositioning was analysed by dissecting it into perpendicular and parallel transposition. Mutants, specific inhibitor and knockdown experiments were further performed to investigate the role of CLIP-170 phosphorylation. Finally, CLIP-170 phosphorylation relation to T cell activation was examined using qPCR to quantitate the IL-2 expression.

2.2 Material and methods

2.2.1 Reagents

The following antibodies were purchased: anti-CD3ε (BD Pharmingen), anti-CD28 (BD Pharmingen) and anti-CD45 (Abcam). Phosphate-buffered saline (PBS) and low fluorescence medium (LFM) for cell culture work were prepared in accordance to the following composition:

PBS-

10 mM Na_2HPO_4 (Wako), 1.76 mM KH_2PO_4 (Wako), 137 mM NaCl (Wako) and 2.7 mM KCl (Wako).

Low fluorescence medium (LFM)

MEM essential amino acid solution (Invitrogen) 10 ml, MEM non-essential amino acid solution 100 × (Invitrogen) 5 ml 10% Glucose (Wako) 5 ml, Glutamine 100 × (Invitrogen) 5 ml, 1% $CaCl_2$ (Wako) 10 ml, 1% $MgSO_4$ (Wako) 20 ml, 0.5% KCl (Wako) 50 ml, 6.8% NaCl (Wako) 50 ml, 0.14% $NaH_2PO4 \cdot 2H_2O$ (Wako) 50 ml, 7.5% Sodium Bicarbonate (Invitrogen), Choline Chloride (Wako) 0.5 mg, Inositol (Wako) 1 mg, Nicotinamide (Wako) 0.5 mg, Pyridoxine hydrochloride (Wako) 0.5 mg, Thiamine-HCl (Wako) 0.5 mg and 1 M HEPES buffer (Invitrogen) 12.5 ml. Formulated medium was adjusted to pH 7.4 with 1 M NaOH and sterilized via 0.25 µm bottle top filter (BD Falcon).

2.2.2 Plasmid constructs, cell culture and transfection

Human CLIP-170 was PCR amplified from cDNA fragment prepared from Jurkat T cells (E6-1, ATCC) mRNA using a primer pairs (Table 2.1 primer 1 & 2). The Jurkat T cell mRNA was prepared from TRIzol Plus RNA Purification Kit (Invitrogen). The PCR amplified product were digested (SalI & BamHI) and cloned into the N-terminal site of pEGFP206K-N1 (pmEGFP-N1), a monomeric mutant of pEGFP-N1 (Clontech)[40]. The CLIP-170 and mEGFP were separated by a long and flexible $(GGGGS)_3$ linkers [41,42]. Additionally, CLIP-170 was cloned into TagRFP-T vector, a modified version of TagRFP (Evrogen, Russia) for the CLIP-170-TagRFP-T construct. Additionally, two CLIP-170 mutants were carried out at Ser-312: a S312A phosphodeficient mutation, and a S312D phosphomimetic mutation. Both the S312A and S312D mutants of CLIP-170 were generated by

site directed mutagenesis (SDM) from CLIP-170-$(GGGGS)_3$-mEGFP using two primer pairs (Table 2.1 primer 3 & 4 for S312A; primer 5 & 6 for S312D).

Jurkat T cells were maintained at 37˚C (5% CO_2) in RPMI-1640 (Gibco, USA) supplemented with 10% fetal bovine serum (Gibco), 2 mM glutamine, 50 U/ml penicillin and 50 µg/ml streptomycin (Gibco). Passage on every 3 days at 1/10 dilution were carried out to maintain cell integrity. DNA transfection was performed using NEON electroporation system (Thermo Fisher Scientific) following the standard operation protocol recommended by the manufacturer manual. The electroporation condition was optimized at 1.0 x 10^6 cells, 5 µg of DNA, 1200 V (pulse voltage) and 40 ms (pulse width).

2.2.3 T cell stimulation

For MTOC repositioning analysis, 35-mm glass bottom dishes (MatTek) were incubated overnight at 4˚C with stimulatory or nonstimulatory antibody solution to adsorb antibodies onto the glass bottom surface. The stimulatory antibodies were 1 µg/ml mouse anti-human CD3ε antibody (HIT3a, BD Pharmingen) and 1 µg/ml mouse anti-human CD28 antibody (CD28.2, BD Pharmingen) solution, while the nonstimulatory antibody was 1 µg/ml mouse anti-human CD45 antibody (MEM-28, abcam) solution. The antibody-coated glass dishes can be stored up to a week at 4˚C. Just before imaging, the antibody-coated glass bottom dishes were washed twice with PBS, then Jurkat T cells (1-2 × 10^4 cells) were introduced into the antibody-coated dishes and stimulated by incubation on the dishes at 37˚C for 20 min in an imaging medium (25 mM HEPES and MEM without phenol red, riboflavin, and folic acid). Precaution were taken during the PBS washing of antibody-coated dish by pipetting gently at the edge of glass surface to prevent absorbed antibody detach from the glass surface. For qPCR experiments, all the preparations procedures for antibody-coated dishes were carried out the same manner but Jurkat T cells were stimulated for 24 hours on the antibody-coated culture dishes at 37˚C.

2.2.4 MTOC repositioning analysis

Jurkat cells were imaged at 37˚C using an inverted microscope (IX71, Olympus) equipped with an infinity-corrected objective (PlanApo 100× NA 1.40 oil TIRFM, Olympus, Japan), optical filters (U-MCFPHQ, Olympus), and the temperature control system (Tokai Hit). GFP and RFP were excited with a 490-nm light-emitting diode (LED) and a 535-nm LED, respectively (pE-2, CoolLED). Fluorescence images were captured with a cooled CCD camera (C10600-10B, Hamamatsu Photonics) controlled by MetaMorph (Molecular Devices, Japan).

The distance between the MTOC and the cell surface was measured using the specimen focusing z-stage of the microscope. The corrected distance z was calculated from z-stage mechanical shift z_0 as:

$$z = z_0 \frac{n_{\text{specimen}}}{n_{\text{glass}}}, \qquad (1)$$

where n_{specimen} is the refractive index of the specimen, and n_{glass} is that of the coverslip and immersion oil[38]. We used n_{specimen} of 1.37, that of the cytoplasm of Jurkat cells[50], and n_{glass} of 1.52 that of BK7 and immersion oil.

MTOC centreing at the cell surface during T cell activation was quantified as a fraction of cells whose MTOC was positioned at the centre region. The “centre” and “periphery” regions were divided by an ellipse with a half diameter of the cell of interest (see Fig. 2.1 for details).

2.2.5 Quantitative real-time PCR

Total mRNA from stimulated Jurkat T cells was extracted using PureLink RNA Mini Kit (Life technologies). Relative expression of IL-2 was quantified by qPCR[49]. Quantification of IL-2 mRNA was performed on a Thermal Cycler Dice Real Time System II (Takara) using the One Step SYBR PrimeScript PLUS RT-PCR kit (Takara). The primer pairs are shown in Table 2.2. The PCR mixture contained 2 µl of extracted mRNA, 10 µl of One Step SYBR RT-PCR buffer 4 (2×), 1.2 µl of Takara Ex Taq HS Mix, 0.4 µl of PrimeScript PLUS RTase Mix, primer pairs (optimized to final concentration of 10 µM) and sterile water to a final reaction volume of 20 µl. The optimal cycling conditions were 5 min at 42˚C, 10 s at 95˚C;

40 cycles of 5 s at 95˚C, 30 s at 60˚C. All qPCR reactions were performed in triplicate. Data were normalized against ß-Actin expression, and the IL-2 relative expression was calculated using the comparative C_T method.

2.2.6 Knockdown experiments

Knockdown experiments were performed using expression vectors for short hairpin RNAs (shRNA) targeting human CLIP-170 (Block-iT Pol II miR RNAi Expression Vector Kit, Thermo Fisher Scientific) and the NEON electroporation system (Thermo Fisher Scientific). The shRNA sequences were designed using BLOCK-iT RNAi Designer (Invitrogen, Table 2.3). The cloned CLIP-170 sequences from Jurkat T cell (shCLIP-170 #1) and the reference sequence database (NM_001247997.1, shCLIP-170 #2) were used as references. Prior to use in Jurkat T cells, the knockdown efficiency was confirmed using HeLa cells. The cells were cultured in DMEM supplemented with 10% fetal bovine serum. Transfection of HeLa cells with the knockdown vector was carried out using the NEON electroporation system. After incubation at 37˚C for 24 h, cells were selected with 20 µg/ml blasticidin for 24 h, then the RNA and protein were extracted for qPCR and immunoblotting analysis. The knockdown efficiency of shRNA against CLIP-170 was assessed by qPCR and immunoblotting (Fig. 3.3). According to the knockdown efficiency, the sequence shCLIP170 #1 was used for knockdown experiments in Jurkat T-cells.

Jurkat cells were transfected with the vector carrying shRNA targeting shCLIP-170 #1 with tandemly arranged EmGFP. Simultaneously expressed EmGFP was used for selection of knockdown cells during live cell imaging.

2.2.7 Immunoblotting

Cells were rinsed twice with PBS and lysed in lysis buffer (2 mM EDTA, 10 mM Tris-HCl pH 7.5, 150 mM NaCl, 1% Nonidet P-40) containing protease inhibitors cocktail (0.1% Aprotinin, 3 µg/ml Antipain, 3 µg/ml Cymostatin, 10 µg/ml Leupeptin, 5 µg/ml Pepstatin A and 1 mM PMSF). After 20 min on ice, lysates were cleared by centrifugation at 20,000 × g for 10 min at 4°C. Protein

concentration was measured using bicinchoninic acid protein assay reagent (Pierce). Equal amounts of protein were heated at 95°C for 10 min with 2 × SDS gel loading buffer, and resolved on 7.5% SDS-polyacrylamide gels (Bio-Rad) by electrophoresis at 50 V for 60 min followed by 75 V for 90 min on ice. The proteins were transferred to a polyvinylidene fluoride membrane (Merck Millipore) using TRANS-BLOT semidry transfer cell (Bio-Rad) at 8 mA for 40 min. Immunoblotting was performed using the iBind Western system (Thermo Fisher Scientific) according to manufacturer's instructions. The following antibodies were use: anti-CLIP-170 (ab134907, abcam), anti-GAPDH (sc-47724, Santa Cruz), HRP-conjugated anti-mouse IgG (G21040, Invitrogen) and HRP-conjugated anti-rabbit IgG (G21234, Invitrogen). The signal was detected using SuperSignal West Dura Extended Duration substrate (Pierce) and ImageQuant LAS-4000 mini imager (GE Healthcare).

Table 2.1. Primers used for plasmid preparations

Primers for CLIP-170	
1	Forward 5'-AGCTGTCGACGCCACCATGAGTATGCTAAAGCCAAGTGGGC-3'
2	Reverse 5'-CAACTGCAATGACGACGAAACCTTCGGGGATCCAGCT-3'
Primers for site-directed mutagenesis of S312A mutant of CLIP-170	
3	Forward 5'-CGCAGCCCTGCTGCCTCTTCCCTCAG-3'
4	Reverse 5'-CTGAGGGAAGAGGCAGCAGGGCTGCG-3
Primers for site-directed mutagenesis of S312D mutant of CLIP-170	
5	Forward 5'-CGCAGCCCTGATGCCTCTTCCCTCAG-3'
6	Reverse 5'-CTGAGGGAAGAGGCATCAGGGCTGCG-3'

Table 2.2. Primers for qPCR (quantitative real-time PCR)

Primers for RT-PCR of IL-2 (relative expression of IL-2)	
3	Forward 5'-GCATTGCACTAAGTCTTGCAC-3'
4	Reverse 5'- TCCTGGTGAGTTTGGGATTC-3'
Primers for RT-PCR of ß-Actin (control, relative expression of IL-2)	
5	Forward 5'-AGAGCTACGAGCTGCCTGAC-3'
6	Reverse 5'-AGCACTGTGTTGGCGTACAG-3'
Primers for RT-PCR of CLIP-170 (knockdown efficiency)	
1	Forward 5'-CAGTGGGCTGGAATTGTTTT-3'
2	Reverse 5'-GTCTGCAGGCCATTAGCTTC-3'

Table 2.3. Short hairpin RNAs (shRNAs) used for CLIP-170 knockdown

CLIP-170 shRNA #1	
1	Sense 5'-TGCTGCTTAGTGCCACCAACCAATACGTTTTGGCCACTGACTGACGT ATTGGTGTGGCACTAAG-3'
2	Antisense 5'-CCTGCTTAGTGCCACACCAATACGTCAGTCAGTGGCCAAAACGTATT GGTTGGTGGCACTAAGC-3'
CLIP-170 shRNA #2	
3	Sense 5'-TGCTGATCAGCTGCTCTTCTCTCTCAGTTTTGGCCACTGACTGACTGA GAGAGGAGCAGCTGAT-3'
4	Antisense 5'-CCTGATCAGCTGCTCCTCTCTCAGTCAGTCAGTGGCCAAAACTGAGA GAGAAGAGCAGCTGATC-3'
Control shRNA	
5	Sense 5'-TGCTGAAATGTACTGCGCGTGGAGACGTTTTGGCCACTGACTGACGT CTCCACGCAGTACATTT-3'
6	Antisense 5'-CCTGAAATGTACTGCGTGGAGACGTCAGTCAGTGGCCAAAACGTCTC CACGCGCAGTACATTTC-3'

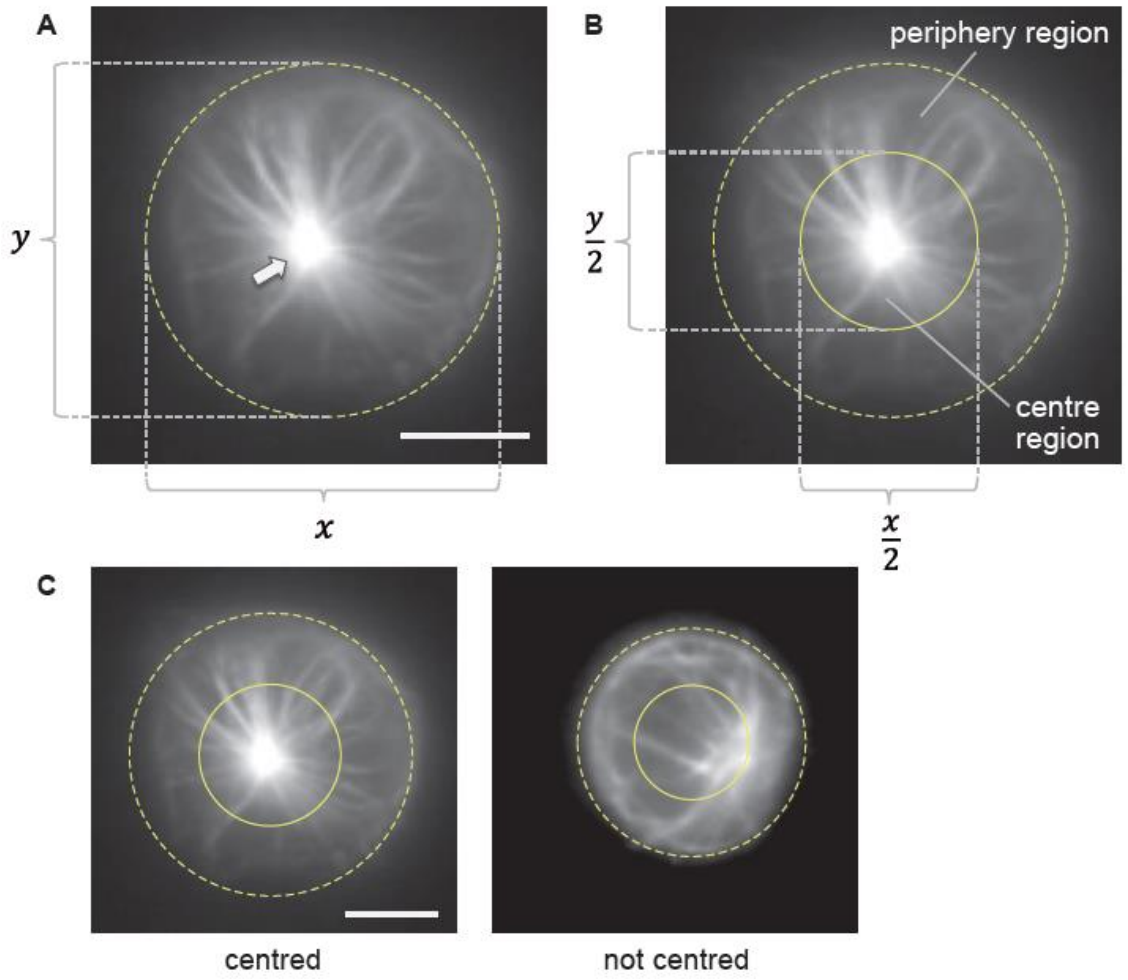

Figure 2.1 Quantification of MTOC centreing. Centreing was quantified as a fraction of cells whose MTOC positioned to the centre region. The "centre" and "periphery" regions were divided by an ellipse with a half diameter of the cell of interest. (**A**) The diameters of the cell were determined by approximating the cell contour to an ellipse with diameters x and y in the x- and y-direction, respectively. The arrow indicates MTOC. (**B**) The boundary between the "centre" and "periphery" region was defined as an ellipse with the half diameters x/2 and y/2 in the x- and y-direction, respectively. (**C**) MTOCs were scored as "centred" if they reside at the "centre" region. They were scored as "not centred" if they reside at the "periphery" region, and were scored also as "not centred" if they resides on the boundary or they are not clearly imaged. Scale bar, 5 µm.

2.3 Results

2.3.1 CLIP-170 regulates MTOC repositioning and T cell activation

2.3.1.1 MTOC repositioning is composed of two directional transpositions: perpendicular and parallel to the contact surface

To visualise and quantify the molecular interactions and dynamics of proteins underlying MTOC repositions, a simultaneous dual-colour fluorescence microscope was used. The microscope was equipped with an illumination system that enable switching among total internal reflection fluorescence (TIRF), highly inclined and laminated optical sheet (HILO), and epi-fluorescence microscopy[37,38]. Jurkat T cells were costimulated with anti-CD3ε and anti-CD28 antibodies coated on glass bottom dishes. This costimulation induces full activation of T cell signalling[39]. In control experiments, T cells remained unstimulated on glass-bottom dishes coated with an anti-CD45 antibody. The full activation of Jurkat T cells by costimulation was confirmed by quantitating the IL-2 expression using qPCR (Fig. 2.2).

We first visualised microtubules using CLIP-170-TagRFP-T. As CLIP-170 binds only at the growing plus-end of microtubule, the dynamic movement of microtubules can be clearly visualised as characteristic comet-like structures of CLIP-170. MTOCs were visualised by epi-fluorescence microscopy at a plane where the bright spot of MTOC was focused (Fig. 2.3A and B bottom). Imaging at the cell surface of contact by TIRF was used to measure the distance of the MTOC from the contact surface (Fig. 2.3A and B top).

Two quantities were measured to dissect MTOC repositioning into two directions, perpendicular and parallel to the contact surface (Fig. 2.3C and D, Table 2.4):

- The perpendicular direction was defined as the MTOC distance from the contact surface, calculated from the focusing shift and corrected for the refraction at the contact surface[38].
- The parallel direction was defined as the MTOC centreing fraction, quantified as the fraction of cells whose MTOC was positioned at the centre

region (i.e. the immunological synapse). The centre and periphery region was defined by dividing the cell surface by an ellipse with half of the diameter of the cell of interest (Fig. 2.1).

Comparison between the stimulated and unstimulated Jurkat cells showed that MTOC repositioning is composed of both transpositions: perpendicular transposition closer to the contact surface (Fig. 2.3C) and parallel transposition into the centre region (Fig. 2.3D).

2.3.1.2 CLIP-170 knockdown impairs MTOC repositioning and full activation of T cells upon stimulation

To assess the functional contribution of CLIP-170 to MTOC repositioning, CLIP-170 knockdown experiments were performed. Vectors carrying shRNA targeting CLIP-170 with tandemly arranged EmGFP was constructed and transfected into Jurkat cells together with TagRFP-T-MAP4, which was used for visualisation of microtubules and MTOCs. Knockdown efficiency of shRNA used for live cell imaging was confirmed using quantitative real-time PCR (qPCR) (Fig. 2.4A) and immunoblotting experiments (Fig. 2.4B). Only knockdown cells were observed using simultaneously expressed EmGFP. Fluorescence images of TagRFP-T-MAP4 in CLIP-170 knockdown cells stimulated with the coated anti-CD3ε/anti-CD28 antibodies showed disturbed microtubule frameworks and decentred the MTOC position (Fig. 2.5A and B). The MTOC centreing fraction in CLIP-170 knockdown cells was significantly decreased compared with wild-type cells ($p = 0.028$) (Fig. 2.5C, Table 2.5), which was consistent with the previously reported results on B cells[12]. Further, the degree of T cell activation was assessed by IL-2 expression, which was quantitated by qPCR. The relative IL-2 expression in CLIP-170 knockdown cells decreased significantly compared to that in the wild-type cells ($p = 0.036$) (Fig. 2.5D, Table 2.5). It is noteworthy that the presence of endogenous CLIP-170 counteracts the knockdown effect. Taken together, CLIP-170 knockdown impaired MTOC repositioning and the full activation of T cells upon stimulation.

2.3.1.3 An AMPK inhibitor, compound C (CC) impairs MTOC repositioning and full activation of T cells upon stimulation

Next, the functional connectivity of CLIP-170 phosphorylation in MTOC repositioning was assessed. CLIP-170 is phosphorylated by AMPK[36], and AMPK mediates IL-2 expression upon T cell stimulation[40]. Fluorescence imaging of MTOCs and microtubules using TagRFP-T-MAP4 showed that an AMPK inhibitor, compound C[41], also disturbed microtubule frameworks and decentred the MTOC position (Fig. 2.6A and B). The MTOC centreing fraction of cells in the presence of compound C was significantly decreased compared with that in the absence of this compound ($p = 0.005$) (Fig. 2.6C, Table 2.5). The relative expression of IL-2 in the presence of compound C decreased significantly compared to that in the absence of this compound ($p < 0.001$) (Fig. 2.6D, Table 2.5). In contrast, the TCR/CD3 microclusters were clearly observed in the presence and absence of compound C in T cells (Fig. 2.7A and B), shows that compound C had no effect on TCR/CD3 microcluster formation upon stimulation. This observation indicates that CLIP-170 phosphorylation by AMPK is not involved in TCR signalling interactions during the initial stages of the activation. Collectively, these results indicate that phosphorylation of CLIP-170 mediates both MTOC repositioning and full activation of T cells upon stimulation.

2.3.2 CLIP-170 S312 phosphorylation is responsible for MTOC repositioning and T cell activation

2.3.2.1 A phosphodificient S312A mutant of CLIP-170 impairs MTOC repositioning and full activation of T cells, but a phosphomimetic S312D mutant does not

To clarify the roles of CLIP-170 phosphorylation in MTOC repositioning, we generated two human CLIP-170 mutants with substitutions at Ser-312, which is the target residue of AMPK[36], a phosphomimetic S312D mutant and a phosphodeficient S312A mutant .

At first, to confirm that S312 is phosphorylated, the C-terminal mEGFP-tagged proteins of the wild-type CLIP-170, and the S312D mutant, co-expressed with TagRFP-T-MAP4 in Jurkat T cells were imaged with the presence of compound C (Fig. 2.8A and B). As shown in Fig. 3.7C, S312D mutation rescued the impaired MTOC centreing caused by AMPK inhibition (Fig. 2.6C). It is noteworthy that stimulated S312D mutant exhibits the similar MTOC centreing as wild-type (Fig. 2.8D) in the presence (Fig. 2.8B) or absence (Fig. 2.9A and B) of compound C. The relative IL-2 expression in cells with S312D mutant also exhibit the similar expression to the wild-type cells upon stimulation (Fig. 2.9C). This observation suggests that most of the endogenous CLIP-170 was phosphorylated by AMPK.

Further, the effect of phosphodeficient mutation in S312 was checked. mEGFP-tagged proteins of the wild-type CLIP-170 and S312A mutants co-expressed with TagRFP-T-MAP4 were imaged (Fig. 2.8D and E). The phosphodeficient S312A mutant CLIP-170 showed disturbed microtubule frameworks and decentred the MTOC position. The centreing fraction was largely and significantly decreased in the phosphodeficient S312A mutant ($p = 0.001$) (Fig. 2.8F, Table 2.6). The relative IL-2 expression in cells with the S312A mutant decreased significantly compared to the wild-type cells ($p = 0.013$) (Fig. 2.8G, Table 2.6). Taken together, these results demonstrate that phosphodificient S312A mutant of CLIP-170 impairs MTOC repositioning and full activation of T cells upon stimulation, but phosphomimetic S312D mutant does not. Thus, the effect of CLIP-170 Ser-312 phosphorylation was clearly shown.

2.3.2.2 MTOC centreing requires phosphorylated CLIP-170 at Ser-312, while MTOC distance from the surface is caused solely by stimulation

To check the difference between the roles of CLIP-170 phosphorylation and T cell stimulation, the MTOC distance and centreing fraction were quantitated. Fluorescence images of S312A mutant CLIP-170-TagRFP-T in stimulated Jurkat cells (Fig. 2.10A) was quantified (Fig. 2.10B and C), and compared with those of wild-type CLIP-170-TagRFP-T in stimulated cells and unstimulated cells (Fig. 2.3A–D). The MTOC distance from the contact surface of the S312A mutant in stimulated cells (1.1 ± 0.6 µm) was not significantly different from that of wild-type CLIP-170 in stimulated cells (0.9 ± 0.3 µm, $p = 0.07$) (Fig. 2.10B, Table 2.4). In contrast, the MTOC distance from the contact surface of wild type CLIP-170 in stimulated cells and in unstimulated cells (2.1 ± 1.3 µm) showed a significant difference ($p < 0.001$). This data demonstrates that S312A and wild-type CLIP-170 show similar MTOC distance from the contact surface upon stimulation, but unstimulated cells do not.

On the contrary, the MTOC centreing fraction of the S312A mutant in stimulated cells is largely and significantly decreased compared with that of the wild-type in stimulated cells ($p = 0.001$), and was not significantly different from that of the wild-type in unstimulated cells ($p = 0.47$) (Fig. 2.10C, Table 2.4). This data show that the S312A mutant impairs the MTOC centreing fraction compare to that of wild-type CLIP-170 in T cells upon stimulation. Together with the data on MTOC distance from the contact surface, these findings indicate that:

(1) MTOC parallel transposition, centreing, requires phosphorylated CLIP-170 at Ser-312

(2) MTOC perpendicular transposition closer to the surface is caused solely by stimulation without CLIP-170 phosphorylation

(3) Consequently, MTOC repositioning and full activation of T cells require both CLIP-170 phosphorylation and T cell stimulation.

Table 2.4 The MTOC distance from the cell surface of contact (source data for Figs. 2.3C,D & 2.10B,C)

	MTOC distance z from the contact surface[a] (μm)	MTOC centreing (%)	N_{cell}
WT (stimulated)	0.94 ± 0.31	79.2 ± 7.2	37
WT (unstimulated)	2.14 ± 1.26	20.4 ± 14.9	25
S312A (stimulated)	1.15 ± 0.59	28.2 ± 8.1	25

Data are mean ± standard deviation (SD). N_{cell} indicates the number of cells.
[a] The MTOC distance z from cell surface was corrected using Equation 1.

Table 2.5 The fraction of MTOC centreing and IL-2 relative expression (source data for Fig. 2.5C,D & 2.6C,D)

	MTOC centreing (%)	N_{cell}	IL-2 relative expression[a]
shControl (stimulated)	60.7 ± 3.0	37	1 [b]
shCLIP-170 (stimulated)	46.5 ± 7.5	43	0.72 ± 0.1
Vehicle (stimulated)	80.9 ± 5.2	47	1 [b]
CC (stimulated)	42.3 ± 11.5	52	0.49 ± 0.1

Data are mean ± SD. N_{cell} indicates the number of cells.

[a] The relative expression of IL-2 was quantified by qPCR in triplicate.

[b] Normalised to the data from this reference gene.

Table 2.6 The fraction of MTOC centreing and IL-2 relative expression (source data for Fig. 2.8C,F,G)

	MTOC centreing (%)	N_{cell}	IL-2 relative expression[a]
WT	81.6 ± 2.0	25	1 [b]
S312A	33.3 ± 9.2	42	0.61 ± 0.1
WT/CC	39.1 ± 1.9	64	
S312D/CC	77.8 ± 1.9	27	

Data are mean ± SD. N_{cell} indicates the number of cells.

[a] The relative expression of IL-2 was quantified by qPCR in triplicate.

[b] Normalised to the data from this reference gene.

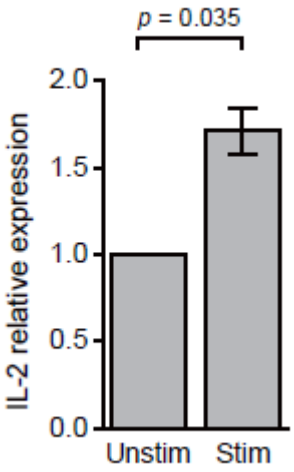

Figure 2.2 Real-time RT-PCR analysis of IL-2 gene expression in stimulated Jurkat cells. Cells were incubated on the anti-CD3ε/anti-CD28 (stimulatory) or anti-CD45 (nonstimulatory) antibody coated dishes for 24 h, then the total RNA was extracted and subjected to qPCR analysis of IL-2. Data shown are the mean fold change ± SD of three independent experiments.

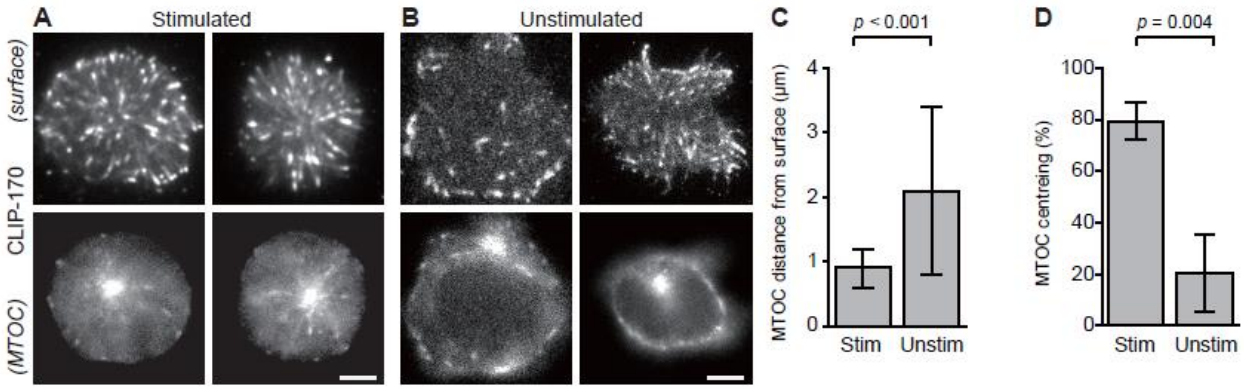

Figure 2.3 MTOC repositioning is composed of two directional transpositions: perpendicular and parallel to the contact surface. (**A–D**) MTOC repositioning is composed of transpositions in two directions, perpendicular and parallel to the contact surface. Fluorescence live-cell imaging of CLIP-170-TagRFP-T (**A,B**) expressed in Jurkat T cells, visualised by TIRF at the surface of contact (top) and by epi-fluorescence microscopy at the plane containing MTOC (bottom), stimulated with the anti-CD3ε/anti-CD28 antibodies (**A**) and unstimulated with the control anti-CD45 antibody (**B**) coated glass bottom dishes. Perpendicular transposition quantified as the MTOC distance from the contact surface (**C**), and parallel transposition quantified as MTOC centreing, the fraction of cells whose MTOC was positioned at the centre region (**D**), analysed using the fluorescence images. Cells were stimulated at 37°C for 20 min with the coated antibodies, followed by imaging at 37°C in all observations. Bars, 5 µm. Data are means ± standard deviation (SD). Source data, Tables 2.4. p, p-values; NS, not significant; stim, stimulated; unstim, unstimulated.

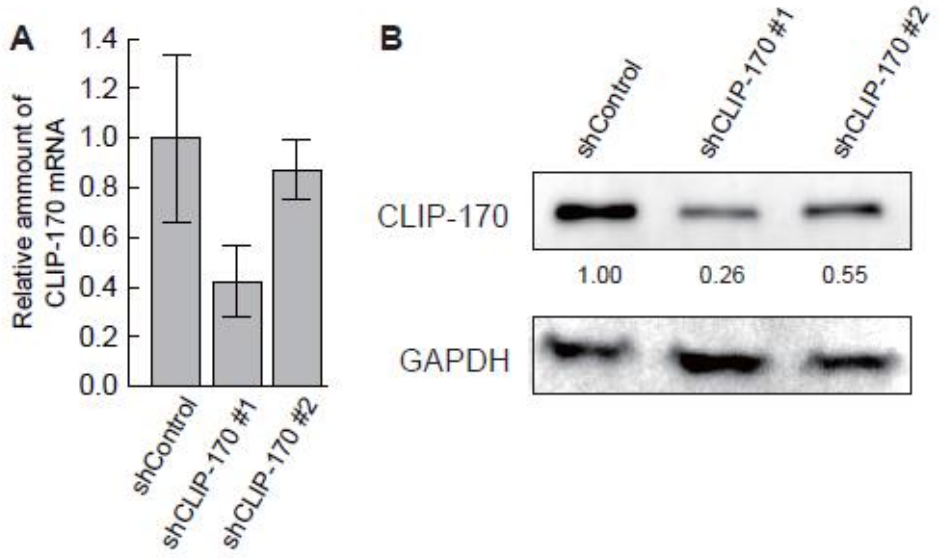

Figure 2.4 The knockdown efficiency of shCLIP-170. The knockdown plasmids were transfected into HeLa cells and selected with blasticidin (20 mg/mL, 24-48 h after transfection), then the total RNA and protein were extracted. The cloned CLIP-170 sequences from Jurkat T cell (shCLIP-170 #1) and the reference sequence database (NM_001247997.1, shCLIP-170 #2) were used as references in shRNA design. (**A**) Reduced amount of CLIP-170 mRNA was confirmed with qPCR. The data indicate the relative mRNA amount ± SD of technical triplicates. (**B**) Protein expression of CLIP-170 was assessed by immunoblotting analysis. Values below the blot represent the relative band intensity compared to shControl after normalization to GAPDH. The sequence of shCLIP170 #1 was used for knockdown experiments in Jurkat T-cells, since it showed higher knockdown efficiency.

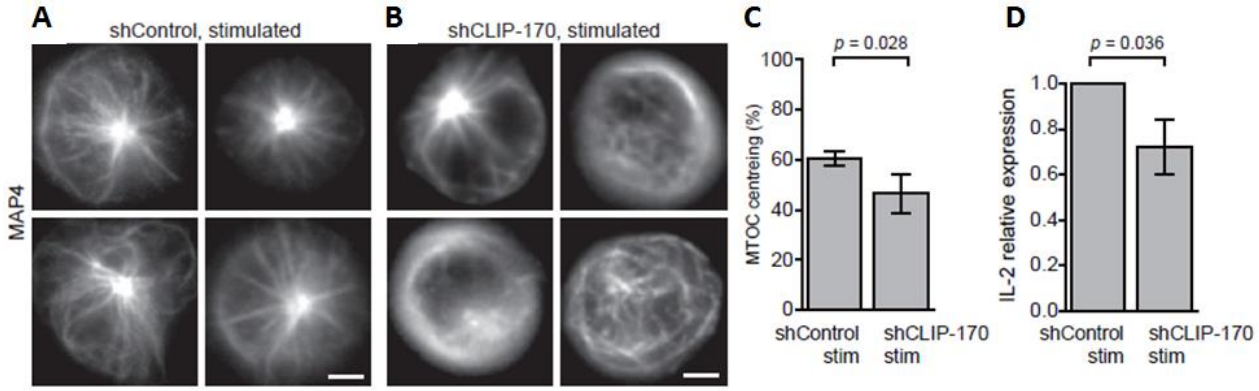

Figure 2.5 CLIP-170 knockdown impairs MTOC repositioning and full activation of T cells upon stimulation. MTOC localisation and microtubule frameworks visualised by epi-fluorescence live-cell microscopy using TagRFP-T-MAP4 (**A,B**) in stimulated Jurkat cells expressing control shRNAs (**A**) and CLIP-170 shRNAs (**B**). MTOC centreing (**C**), and the relative expression of IL-2 (**D**) quantified by qPCR in CLIP-170 shRNA-knockdown or control shRNA-expressing Jurkat cells stimulated on dishes. Cells were stimulated at 37°C for 20 min with the coated antibodies, followed by imaging at 37°C in all observations. Bars, 5 µm. Data are means ± standard deviation (SD). Source data, Tables 2.5. *p*, *p*-values; NS, not significant; stim, stimulated; unstim, unstimulated.

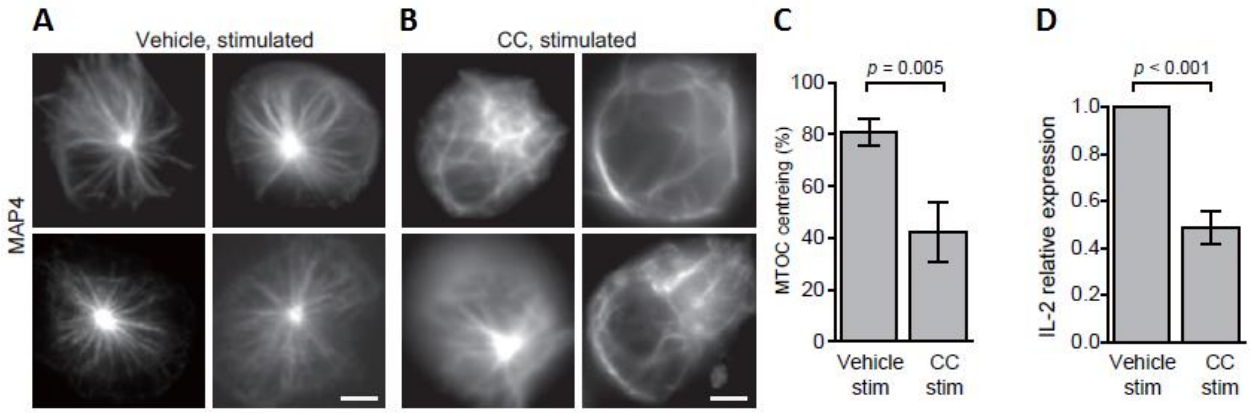

Figure 2.6 The AMPK inhibitor compound C (CC) impairs MTOC repositioning and full activation of T cells upon stimulation. MTOC localisation and frameworks visualised in the same manner as in panels A and B (**A,B**) in the presence of vehicle alone (0.2% DMSO, A) or 20 µM compound C (**B**) in stimulated Jurkat cells. MTOC centreing (**C**), and the relative expression of IL-2 in the presence of vehicle or 20 µM compound C (**D**) in stimulated Jurkat cells. Cells were stimulated at 37°C for 20 min with the coated antibodies, followed by imaging at 37°C in all observations. Bars, 5 µm. Data are means ± standard deviation (SD). Source data, Tables 2.5. p, p-values; NS, not significant; stim, stimulated; unstim, unstimulated.

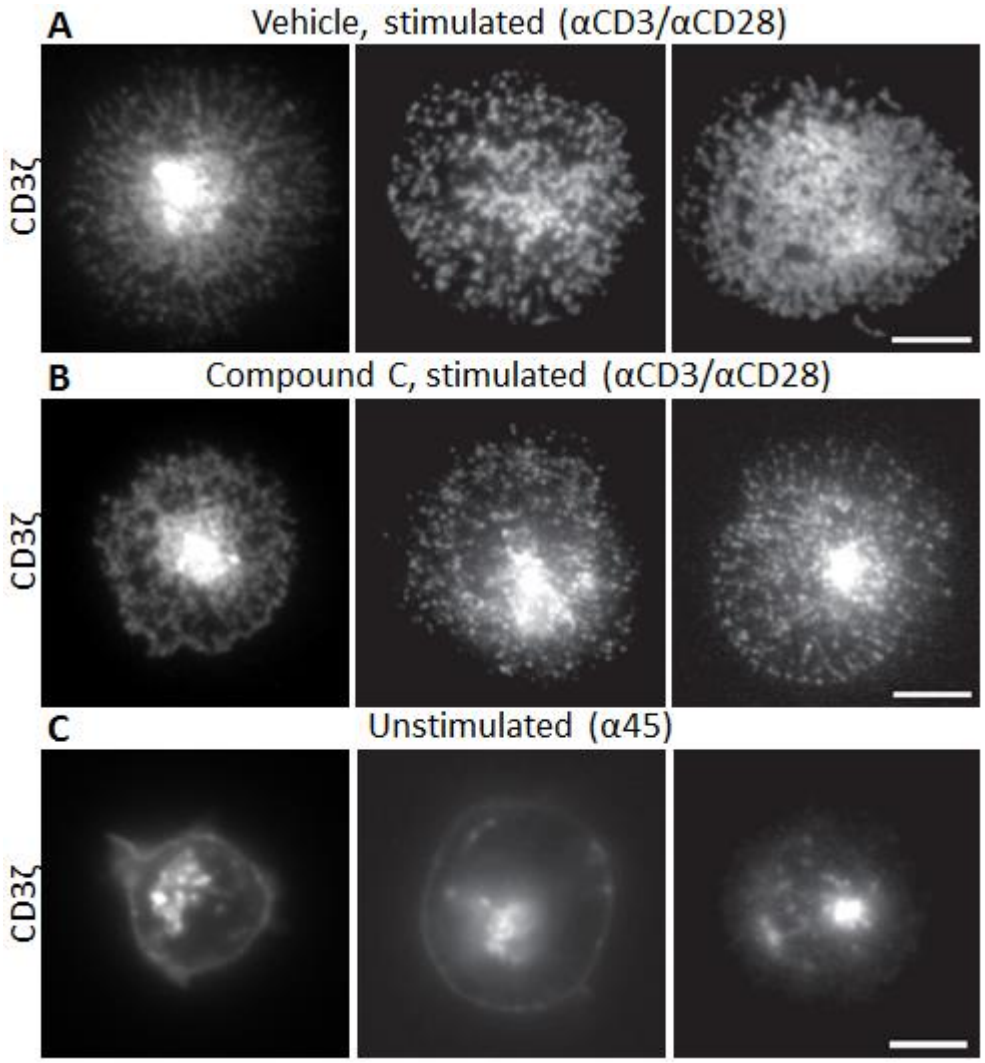

Figure 2.7 Compound C does not inhibit TCR/CD3 microcluster formation. TIRF live-cell imaging of the TCR/CD3 complex at the contact surface in Jurkat T cells expressing CD3ζ-TagRFP-T in the presence of vehicle alone (0.2% DMSO, **A**) or 20 μM compound C (**B**) stimulated with the anti-CD3ε/anti-CD28 antibodies coated on glass bottom dishes, and in unstimulated Jurkat cells expressing CD3ζ-TagRFP-T (**C**) incubated on the control anti-CD45 antibody-coated dishes. Cells were stimulated at 37°C for 20 min with the coated antibodies, followed by imaging at 37°C in all experiments. Scale bar, 5 μm.

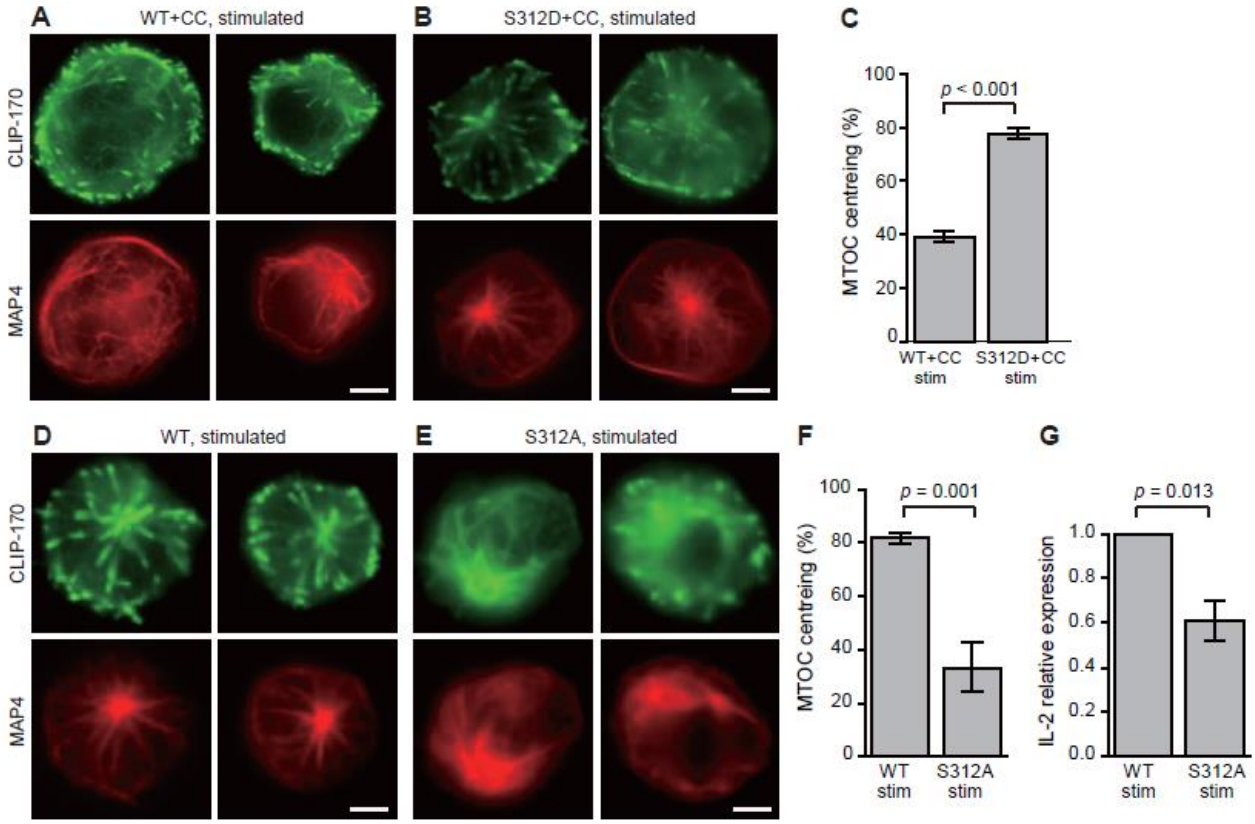

Figure 2.8 A phosphodeficient S312A mutant of CLIP-170 impairs MTOC repositioning and full activation, and a phosphomimetic S312D mutant does not. Dual-colour epi-fluorescence live-cell imaging (**A**,**B**,**D** and **E**) at the contact surface in stimulated Jurkat cells using combinations of TagRFP-T-MAP4 (red, bottom) with C-terminal mEGFP-tagged proteins (green, top): wild-type CLIP-170 in the presence of 20 µM compound C (**A**), phosphomimetic S312D mutant (**B**) in the presence of 20 µM compound C, wild-type CLIP-170 (**D**) and phosphodeficient S312A mutant (**E**). MTOC centreing (C,F and G) in Jurkat cells expressing wild-type- or S312D-mEGFP in the presence of 20 µM compound C (**C**) and wild-type or G312A-mEGFP (**F**). The relative expression of IL-2 (**G**) in Jurkat cells expressing wild-type or S312A CLIP-170. Bars, 5 µm. Data are means ± SD. Source data, Tables 2.6.

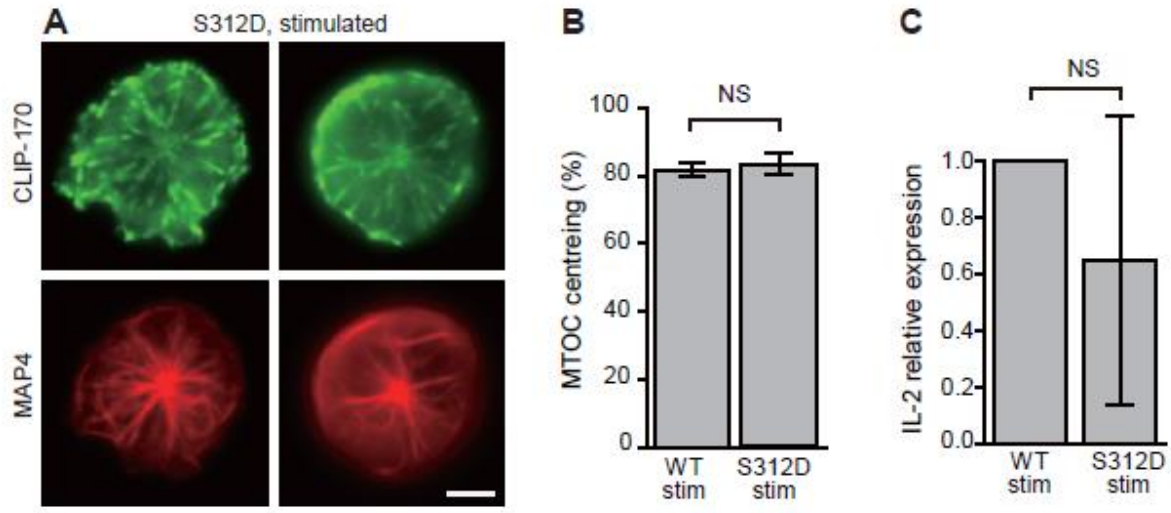

Figure 2.9 CLIP-170 S312D phosphomimetic mutation does not affect either MTOC repositioning or IL-2 expression. (**A**) Jurkat T cells expressing both mEGFP tagged CLIP-170 S312D and TagRFP-T-MAP4 were stimulated by incubation on the anti-CD3ε/anti-CD28 surface, then the images were captured. Protein distribution was similar to wild type. Bar, 5 μm. (**B**) MTOC centreing of MAP4 was measured as described in Figure 2.1. (**C**) The total RNA was extracted from mEGFP tagged CLIP-170 S312D expressing Jurkat T cells, and the relative IL-2 expression was quantified by qPCR.

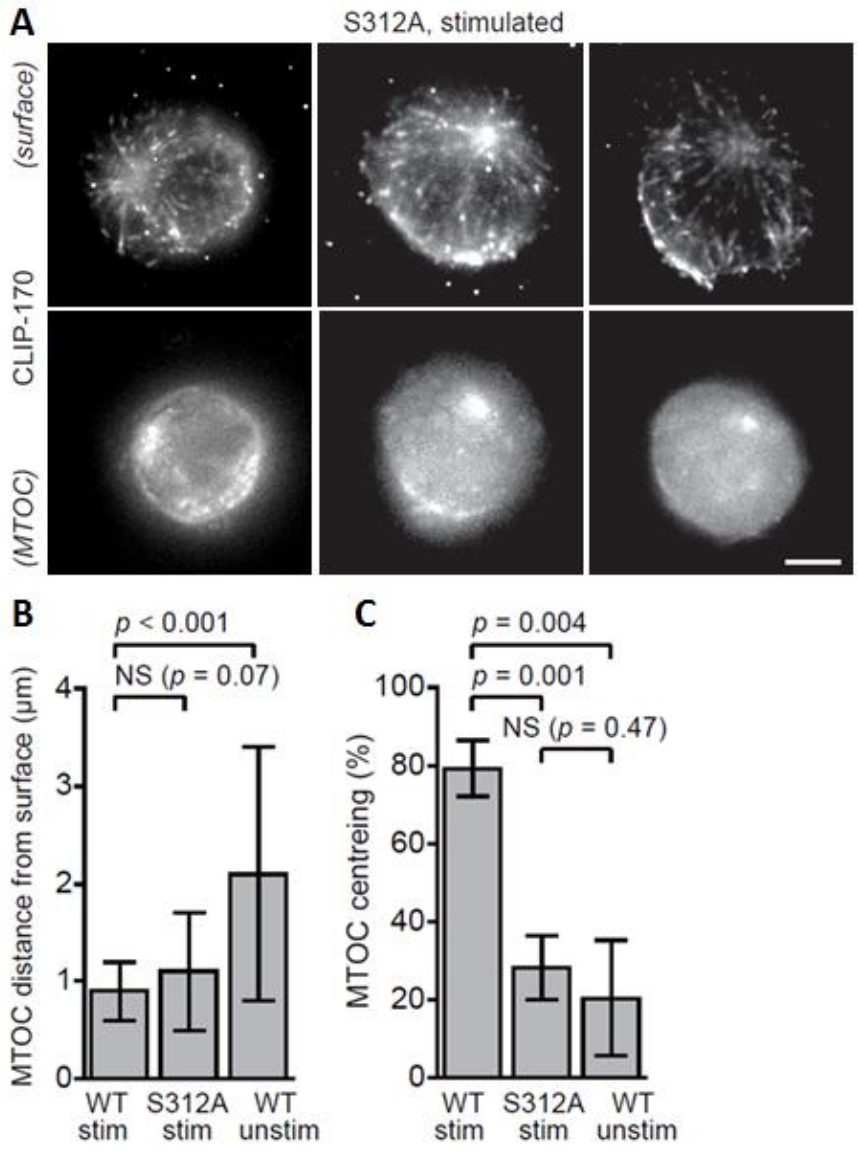

Figure 2.10 MTOC centreing requires phosphorylated CLIP-170 at Ser-312, while MTOC distance from the surface is caused solely by stimulation. TIRF live-cell imaging of S312A-TagRFP-T (A) at the contact surface (top) and by epi-fluorescence at the plane containing MTOC (bottom) in stimulated Jurkat cells. MTOC distance from the surface (B), and MTOC centreing (C), quantified using the images. In panels B and C, the data in Fig. 2.3C and 2.3D are re-plotted for comparison. Bars, 5 µm. Data are means ± SD. Source data, Tables 2.4.

2.4 Discussion

In this chapter, the event of MTOC repositioning in T cell was shown to consist of perpendicular and parallel directional transpositions. Both directional transpositions play crucial roles in regulating the relocation of MTOC towards the contact surface (perpendicular) and at the centre of the interacting interface (parallel).

The perpendicular transposition, defined as the distance of MTOC from the cell surface, is mediated solely by stimulation. With regards to the CLIP-170 inhibition by knockdown experiments, site directed mutagenesis (SDM) or specific inhibitor (compound C), the MTOCs in T cells were still able to reposition perpendicularly closer to cell surface upon stimulation. This clearly shows that the perpendicular transposition of MTOC only requires cell stimulation for the repositioning event to take place.

On the contrary, the parallel directional transposition, defined as the centreing of MTOC at the cell surface, is mediated by CLIP-170 phosphorylation. Inhibition of CLIP-170 phosphorylation by compound C impaired MTOC centreing at the contact surface. Consistently, a CLIP-170 phosphodeficient mutant, SDM on Ser-312, significantly impaired the MTOC centreing fractions in T cell upon stimulation. Taken together, MTOC repositioning to the centre of cell surface in T cell is regulated by CLIP-170 phosphorylation and cell stimulation.

Meanwhile, the MTOC repositioning data also corresponds well to the data on full activation of T cell, where CLIP-170 phosphorylation and cell stimulation were also responsible for full activation of T cell, indicated by the increased in IL-2 expression. Thus, the full activation of T cell is also regulated by CLIP-170 phosphorylation and T cell stimulation.

Although this chapter demonstrates that CLIP-170 phosphorylation and T cell stimulation are important contributing factors for MTOC repositioning and full activation of T cell, the machinery involving CLIP-170 molecular regulation in MTOC repositioning remains elusive. Specifically, the role of CLIP-170 in regulating its partnering proteins during T cell activation is yet to be tested. Further studies involving CLIP-170 and its interacting partners will be critical to provide further understanding for the mechanism of MTOC repositioning in T cell.

Chapter 3

CLIP-170 up-regulates the microtubule plus-end and dynein dynamics

3.1 Introduction

In chapter 2, CLIP-170 phosphorylation was shown to regulate MTOC repositioning in T cell, which in turn, regulates the full activation of T cell. However, it remains elusive how CLIP-170 regulates MTOC repositioning in T cells upon stimulation. Understanding the mechanism concerning CLIP-170 regulation at its molecular level will provide great insight toward studies on T cell activation. Previous reports have revealed that dynein, a microtubule-associated motor protein is also responsible for MTOC repositioning in T cell[7,9].

Dynein is a minus-end directed motor protein with two heavy chains and several accessory light chains that generate forces by moving laterally along the microtubule lattice[6]. Dynein accumulates at the IS before the repositioning of MTOC takes place[6]. Inhibition of dynein activities impair MTOC repositioning and T cell activation[7,9].

To unravel the molecular mechanism of CLIP-170 roles in regulating MTOC repositioning, simultaneous dual-colour live cells imaging was performed for CLIP-170 and proteins that potentially interact with it, specifically dynein to investigate the interplay between these molecules.

In this chapter, the role of CLIP-170 phosphorylation toward microtubule polymerization was first studied using site directed mutagenesis and knockdown experiments, coupled with quantitative microscopy. CLIP-170 and dynein interplay in T cell upon stimulation was further examined. Dynein localisation at the cell surface was found to be critically dependent on CLIP-170. Based on the evidences and data in this study, a model for MTOC repositioning was proposed.

3.2 Material and methods

3.2.1 Plasmid development for DLC, dynactin & CD3ζ

Human dynein light chain (DLC) and dynactin were PCR amplified from cDNA fragment prepared from Jurkat T cell mRNA using two primer pairs (Table 3.1 primer 1 & 2 for DLC; primer 3 & 4 for dynactin). PCR amplified DLC and dynactin were cloned into the pmEGFP-N1 vector. The DNA sequences for DLC and dynactin plasmids were confirmed by sequencing. For the CD3ζ-TagRFP-T construct, it was cloned from the cDNA of CD3ζ-EGFP. The CD3ζ-EGFP cDNA was a generous gift from Dr. T. Yokosuka and Dr. T. Saito (RIKEN, Yokohama, Japan)[43].

Jurkat T cells were maintained at 37˚C (5% CO_2) in RPMI-1640 (Gibco, USA) supplemented with 10% fetal bovine serum (Gibco), 2 mM glutamine, 50 U/ml penicillin and 50 µg/ml streptomycin (Gibco). Passage on every 3 days at 1/10 dilution were carried out to maintain cell integrity. DNA transfection was performed using NEON electroporator (Thermo Fisher Scientific) following the standard operation protocol recommended by the manufacturer manual. The electroporation condition was optimized at 1.0 x 10^6 cells, 5 µg of DNA, 1200 V (pulse voltage) and 40 ms (pulse width).

3.2.2 T cell stimulation

For live cell imaging, 35-mm glass bottom dishes (MatTek) were incubated overnight at 4˚C with stimulatory of 1 µg/ml mouse anti-human CD3ε antibody (HIT3a, BD Pharmingen) and 1 µg/ml mouse anti-human CD28 antibody (CD28.2, BD Pharmingen) solution to adsorb antibodies onto the glass bottom surface. For negative control dishes, glass bottom dishes were incubated with nonstimulatory antibody solution of 1 µg/ml mouse anti-human CD45 antibody (MEM-28, abcam) solution. These antibody-coated glass dishes can be stored up to a week at 4˚C. Just before imaging, the antibody-coated glass bottom dishes were washed twice with PBS, then Jurkat T cells (1-2 × 10^4 cells) were introduced into the antibody-coated dishes and stimulated by incubation on the dishes at 37˚C for 20 min in an imaging medium (25 mM HEPES and MEM without phenol red, riboflavin, and folic acid). Precaution were taken during the PBS washing of

antibody-coated dish by pipetting gently at the edge of glass surface to prevent absorbed antibody detach from the glass surface.

3.2.3 Live cell imaging

To record the T cell activation, Jurkat T cells transiently expressing CLIP-170, dynein, dynactin and CD3ζ were observed on the glass bottom dish coated with stimulatory antibodies of anti-CD3ε/anti-CD28.

For the CLIP-170 comet dynamics and colocalisation analysis, cells were imaged using inverted microscope (IX81, Olympus, Japan) equipped with custom-built TIRF and HILO (highly inclined and laminated optical sheet) microscope setup[34,35]. The microscope is equipped with an infinity-corrected objective (PlanApo 100x NA 1.45 oil TIRFM, Olympus, Japan) and a beam from solid-state laser (488 nm and 20 mW; Sapphire 488-20-OPS; Coherent, Japan) for the fluorescent illumination. The microscope optical filters were custom-ordered (Olympus) to include a dichroic mirror (DM488) and emission filters (Em495-545 for EGFP, Em569-624 for TagRFP-T). Images were captured with three electron-multiplying charge-coupled device (EMCCD) cameras (C9100-13, Hamamatsu Photonics, Japan) controlled by AQUACOSMOS software (Hamamatsu Photonics). Jurkat T cells were observed at 37˚C using temperature control system with a stage top incubator and an objective heater (IBC-IU2-YOP/-CB/-LH, MI-IBC-IU2, Tokai Hit, Japan). The magnification difference, shift and rotation between the two colour images were corrected using ImageConverter (Olympus, Japan) based on Bicubic interpolation with two colour images of a 10-μm square lattice (Olympus) captured at the same time.

3.2.4 CLIP-170 comets velocity and length analysis

Kymographs were created using the Multi Kymograph plugin for ImageJ[51]. The path along a microtubule was traced manually with a segmental line, which was then used in turn to generate a linear intensity profile along the path, i.e., the axis of the microtubule for each frame. This linear intensity profile was represented as a row with a single pixel of the line width, and stacked vertically in temporal sequence from top to bottom. It yielded a kymograph as a

two-dimensional image with pitches of 80 nm/pixel along the horizontal space axis and 1 s/pixel along the vertical time axis.

The CLIP-170 comet velocity v was calculated as the slope of the straight lines in trajectories. The CLIP-170 comet length was calculated as follows: the beginning of the comet was determined as the point where fluorescence intensity (a.u.) encountered rapid rise; its end as the point where fluorescence intensity reached baseline[34]. A minimum of 30 comets were analysed for each data set.

3.2.5 Colocalization and movement analysis

The colocalisation and movement directions of protein clusters were analysed using simultaneous dual-colour TIRF live-cell images by ImageConverter (Olympus Software Technology). Protein clusters were selected manually according to the criteria:

(1) diameter is larger than 240 nm (3 pixels)

(2) difference of the image intensity between the cluster and the surrounding is larger than the standard deviation of that of the surrounding

The protein clusters were categorized into “centre” or “periphery” by their localisation at the centre or periphery region, and into “microtubule plus-end-directed”, “microtubule minus-end-directed” or “immobile” by their movement directions. If the protein clusters of the two kinds of proteins in the dual-colour images were kept colocalised and involved in the same movement category during not less than three consecutive frames, they were counted as “colocalised”. A minimum of 100 cluster sets obtained from five cells were analysed for each data set.

Table 3.1. Primers used for DLC and dynactin plasmids preparation

Primers for dynein light chain	
1	Forward 5'-AGCTGCTAGCGCCACCATGTGCGACCGAAAGGCCGTGATCA-3'
2	Reverse 5'-AGCTCCGCGGACCAGATTTGAACAGAAGAATGGCC-3'
Primers for dynactin	
3	Forward 5'-AGCTGCTAGCGCCACCATGGCACAGAGCAAGAGGCACGTGT-3'
4	Reverse 5'-AGCTCCGCGGGGAGATGAGGCGACTGTGAAGCTGG-3'

3.3 Results

3.3.1 CLIP-170 phosphorylation up-regulates plus-end dynamics but T cell stimulation does not

3.3.1 CLIP-170 phosphorylation up-regulates plus-end comet velocity

The effects of CLIP-170 phosphorylation at Ser-312 on microtubule plus-end dynamics were assessed. Microtubule plus-end dynamics and CLIP-170 comets were visualised using C-terminal mEGFP-tagged CLIP-170s. This was done for wild-type CLIP-170 in stimulated cells, phosphodeficient S312A mutant in stimulated cells, and wild-type in unstimulated cells (Fig. 3.1A-C upper). Microtubule plus-end dynamics was analysed using kymographs (Fig. 3.1A-C lower). First, the velocity of microtubule plus-end comet was assessed. It is calculated as the velocity of CLIP-170 comet transposition from the kymographs (Fig. 3.1D, Table 3.2). The CLIP-170 comet velocity of S312A mutant in stimulated cells decreased significantly compared with that of the wild-type in stimulated cells ($p < 0.001$). In contrast, the comet velocity of the wild-type in unstimulated cells was not significantly different from that in stimulated cells ($p = 0.09$). Thus, it shows that phosphorylation of CLIP-170 at Ser-312 up-regulates the plus-end comet velocity, but T cell stimulation does not.

3.3.2 Unphosphorylated CLIP-170 stabilises the microtubule plus-end

Meanwhile, the CLIP-170 comet length was also determined from the rapid rise and baseline of fluorescence intensity as the beginning and the end of comet from the kymograph. The results show that the CLIP-170 comet length of S312A mutant in stimulated cells increased slightly compared with that of wild-types in stimulated cells ($p = 0.048$) (Fig. 3.1E, Table 3.2), while the comet length of the wild-type in unstimulated cells again did not significantly differ from that in stimulated cells ($p = 0.54$), meaning that unphosphorylated CLIP-170 stabilises the microtubule plus-end dynamics, but T cell stimulation does not.

3.3.3 CLIP-170 phosphomimetic S312D mutant disable the compound C inhibition on microtubule plus-end dynamics

Furthermore, in the phosphomimetic S312D mutant the effect of AMPK inhibition by compound C was investigated. This was done for the wild-type CLIP-170, wild-type CLIP-170 in the presence of compound C, and phosphomimetic S312D mutant in the presence of compound C in stimulated cells (Fig. 3.2A-C upper). Microtubule plus-end dynamics was analysed using kymograph (Fig. 3.2A-C lower). The CLIP-170 comet velocity of wild-type in the presence of compound C decreased significantly compared with that of the wild-type in the absence of this compound in stimulated cells ($p < 0.001$) (Fig. 3.2D, Table 3.2). In contrast, the comet velocity of S312D mutant in the presence of compound C was not significantly different from that of the wild-type in stimulated cells ($p = 0.33$). These show that S312D mutant rescues the plus-end comet velocity from compound C inhibition.

Concurrently, the CLIP-170 comet length determined from the kymograph showed that the comet length of the wild-type in the presence of compound C increased slightly compared with that of wild-types in the absence of this compound in stimulated cells ($p = 0.036$) (Fig. 3.2E, Table 3.2). The comet length of S312D mutant in the presence of compound C again did not significantly differ from that in wild-type CLIP-170 in stimulated cells ($p = 0.73$). These show that S312D mutant disable the compound C inhibition on microtubule plus-end length.

Together with the data on S312A mutant, these results indicate that CLIP-170 phosphorylation up-regulates microtubule plus-end dynamics, which is consistent with previous reports[36], but T cell stimulation does not affect this.

3.3.4 Functional changes in dynamics and localisation of CLIP-170 and dynein

3.4.1 Localisations of the clusters of CLIP-170, dynein, dynactin and the TCR/CD3 complex in T cells.

The functional relation between CLIP-170 phosphorylation and T cell stimulation was investigated. Using simultaneous dual-colour TIRF live-cell imaging, we visualised colocalisations and movement of proteins selected from among those potentially interacting with CLIP-170, specifically the dynein light chain (DLC, a subunit of dynein), dynactin, and CD3ζ (a subunit of the TCR/CD3 complex) (Fig 3.3A-F). Jurkat cells coexpressing C-terminal mEGFP-tagged protein and C-terminal TagRFP-T-tagged counter-protein were stimulated with the anti-CD3ε/anti-CD28 antibodies or remained unstimulated with the control anti-CD45 antibody coated on glass bottom dishes.

When the distribution of dynein in Figure 3.3A, B and C were compared, stimulated wild type-CLIP-170 cells (Fig. 3.3A) show dynein clusters accumulated in the inner area. CLIP-170 also localized in the same inner area, suggesting broad colocalisation. In case of stimulated S312A mutant (Fig. 3.3C), dynein is not accumulated in the inner area. The dynein cluster in the unstimulated cell (Fig. 3.3B) distributes more diffusely. It is due to the higher concentration of the non-clustered dynein. These observations suggest that dynein molecules are anchored at the cell surface of the central region after T cell stimulation.

Next, the distribution of dynactin and CD3ζ clusters in stimulated T cells were observed (Fig. 3.3D-F). Dynactin clusters exhibit similar localisation pattern to the wild-type CLIP-170 clusters (Fig. 3.3D). This observation suggestss compelling colocalisation between these molecules. In contrast, the CD3ζ clusters were distributed mainly around the periphery region of T cells (Fig. 3.3E and F), suggesting that colocalisation with CLIP-170 clusters was unlikely (Fig. 3.3E) but a partial one with dynein clusters (Fig. 3.3F).

3.4.2 Coexistence of plus-end- and minus-end-directed dynein at the centre, and increased dynein relocation to the centre requires both stimulation and CLIP-170 phosphorylation

Using the images in Figure 3.3A-E, the fractions of colocalised and non-colocalised clusters and translocation velocities of clusters were quantified separately at the centre or periphery region (Fig. 3.4A-B & 3.5A-C). The cluster fraction was calculated as the percentage of all the cluster fractions located at either the centre or the periphery (total at both regions = 100%).

First, colocalisation and movement of CLIP-170 and dynein were examined (Fig. 3.4A). Comparison among the data from the wild-type CLIP-170 and dynein in stimulated cells, those in unstimulated cells, and the S312A mutant and dynein in stimulated cells showed that:

(1) plus-end-directed dynein is only observed in colocalised dynein with CLIP-170

(2) that is produced by stimulation, especially at the centre

(3) minus-end-directed dynein is increased by stimulation, especially at the centre

(4) colocalised dynein with CLIP-170 requires CLIP-170 phosphorylation

(5) dynein relocation to the centre was largely increased by stimulation and by CLIP-170 phosphorylation

Accordingly, coexistence of plus-end- and minus-end-directed dynein at the centre requires both T cell stimulation and CLIP-170 phosphorylation, and increased dynein relocation to the centre also requires both the stimulation and CLIP-170 phosphorylation. These indicate that:

(1) both the stimulation and CLIP-170 phosphorylation are essential for coexistence of plus-end- and minus-end-directed dynein at the centre region

(2) both plus-end- and minus-end-directed dynein at the centre is necessary for dynein relocation to the centre

(3) together with results from Fig. 3.2-3.9, dynein relocation to the centre is

responsible for MTOC repositioning and full activation of T cells.

3.4.3 CLIP-170 and dynactin clusters showed colocalisation, whereas CLIP-170 and TCR/CD3 clusters revealed no colocalisation, and dynein and TCR/CD3 clusters only showed a partial one

Next, the colocalisation and movement of CLIP-170 and other proteins were quantitated (Fig. 3.4B) in the same approach discussed in Fig. 3.4A. Dynactin clusters exhibit mainly plus-end-directed movement originating from the central region to the periphery region, similar to the clusters movement of wild-type CLIP-170. Majority of CLIP-170 and dynactin clusters showed colocalisation.

In contrast, TCR/CD3 clusters at the centre and at the periphery were all immobile, while the wild-type CLIP-170 clusters exhibit mainly plus-end tracking toward the periphery in T cells upon stimulation. CLIP-170 and TCR/CD3 clusters revealed no colocalisation.

Dynein clusters on the other hand showed minor colocalisation with TCR/CD3 clusters at the centre and at periphery of T cells. Only dynein clusters that were immobile demonstrate colocalisation with TCR/CD3 clusters, but the plus-end- and minus-end-directed dynein clusters do not show colocalisation with TCR/CD3 clusters. Thus, dynein and TCR/CD3 clusters only showed a partial colocalisation.

3.4.4 The velocities of plus-end tracking clusters of CLIP-170, dynactin and dynein light chain (DLC)

Finally, the translocation velocities of the clusters were quantified using the dual-colour images (Fig. 3.5A-C). The velocities of plus-end tracking of non-colocalised wild-type CLIP-170 in both stimulated and unstimulated cells, those of non-colocalised dynactin, and those of colocalised CLIP-170 and dynactin, did not significantly differ both at the centre and at the periphery (average 0.28 ± 0.07 μm/s) (Fig. 3.5A and B, Table 3.3), corresponding well to the microtubule

growth rate reported previously (17.9 ± 7.7 μm/min, equivalent to 0.30 ± 0.13 μm/s in LLCPK1 cells)[42].

Meanwhile, those of colocalised wild-type CLIP-170 and dynein, and those of S312A mutant CLIP-170 were slower than those of non-colocalised wild-type CLIP-170 (Fig. 3.5A, Table 3.3). These findings indicate that colocalisation of CLIP-170 with dynactin has no effect on the translocation velocity, while colocalisation of CLIP-170 with dynein acts as a source of resistance to the plus-end tracking. Accordingly, the lifetime of the plus-end-directed dynein cluster colocalised with CLIP-170 was approximately 9 s, almost half of that of the minus-end-directed dynein cluster (Table 3.4).

The velocities of minus-end-directed movement of the clusters were quantified (Fig. 3.5C, Table 3.3). Those of dynein in both stimulated and unstimulated cells, and in cells coexpressed with S312A mutant CLIP-170 did not significantly differ both at the centre and at the periphery. The average velocity was 0.054 ± 0.028 μm/s (Table 3.3). It should be noted that all the cluster of minus-end-directed dynein were non-colocalised with CLIP-170. This velocity is in good accordance with the velocity of dynein measured using single molecule imaging (0.079 ± 0.011 μm/s)[20] at the "weakly processive" state, in which dynein does not make complexes with dynactin and cargos[23]. It is also noteworthy that the velocity is also in good accordance with the velocity of MTOC repositioning, 3.26 ± 0.77 μm/min, equivalent to 0.054 ± 0.013 μm/s, reported previously[9].

Table 3.2 CLIP-170 comet velocities and lengths (source data for Figs. 3.1D,E & 3.2D,E)

	Comet velocity (μm/s)	Comet length (μm)	N_{comet}
WT, stimulated	0.32 ± 0.08	0.99 ± 0.23	30
S312A, stimulated	0.13 ± 0.04	1.10 ± 0.16	30
WT, unstimulated	0.28 ± 0.07	1.03 ± 0.27	30
WT + vehicle, stimulated	0.29 ± 0.06	0.94 ± 0.25	30
WT + CC, stimulated	0.24 ± 0.05	1.11 ± 0.38	30
S312D + CC, stimulated	0.28 ± 0.07	0.96 ± 0.17	30

Data are mean ± SD. N_{comet} indicates the number of comets.

Table 3.3 The velocities of the clusters of CLIP-170, DLC and dynactin (source data for Fig. 3.5A-C)

		Velocity (μm/s)			
		[-]	[+]	$N_{cluster}$	Average C and P
WT CLIP-170, not colocalised	C		0.27 ± 0.08 [e]	25	0.28 ± 0.08
stimulated [a]	P		0.30 ± 0.09 [e]	33	
WT CLIP-170 & DLC, colocalised	C		0.15 ± 0.06 [f]	9	0.15 ± 0.07
stimulated [b]	P		0.15 ± 0.08 [f]	7	
WT CLIP-170, not colocalised	C		0.28 ± 0.06 [e]	13	0.27 ± 0.05
unstimulated [b]	P		0.27 ± 0.03 [e]	9	
WT CLIP-170 & DLC, colocalised	C		ND	–	
unstimulated [b]	P		0.16 ± 0.03 [f]	3	
S312A CLIP-170, not colocalised	C		0.20 ± 0.05	15	0.20 ± 0.05
stimulated [c]	P		0.20 ± 0.06	15	
DLC, not colocalised	C	0.057 ± 0.028		22	0.05 ± 0.03
stimulated [b]	P	0.049 ± 0.029		21	
DLC, not colocalised	C	0.058 ± 0.014		3	0.06 ± 0.03
unstimulated [b]	P	0.059 ± 0.032		11	
DLC, not colocalised	C	0.061 ± 0.032		9	0.05 ± 0.03
S312A, stimulated [c]	P	0.051 ± 0.025		29	
dynactin, not colocalised	C		0.27 ± 0.03 [e]	2	0.26 ± 0.03
stimulated [d]	P		0.26 ± 0.04 [e]	3	[e]
CLIP-170 & dynactin, colocalised	C		0.29 ± 0.08 [e]	13	0.29 ± 0.07
stimulated [d]	P		0.30 ± 0.05 [e]	11	
Average of all [-]		0.054 ± 0.028		95	
Average of [+] [e]			0.28 ± 0.07	109	
Average of [+] [f]			0.15 ± 0.06	19	

Data are mean ± SD. $N_{cluster}$ indicates the number of clusters.

[–] and [+] denote the minus-end-directed movement and plus-end tracking, respectively. WT, S312A, and DLC denote wild-type, phosphodeficient S312A mutant, and dynein light chain, respectively. C and P denote the centre and periphery region, respectively.

[a] Data from TIRF images using Jurkat cells co-expressing DLC-mEGFP and wild-type CLIP-170-TagRFP-T, those co-expressing dynactin-mEGFP and wild-type CLIP-170-TagRFP-T, and those co-expressing CD3ζ-mEGFP and wild-type CLIP-170-TagRFP-T stimulated on antibody-coated dishes.

[b] Data from TIRF images using Jurkat cells co-expressing DLC-mEGFP and wild-type CLIP-170-TagRFP-T stimulated and unstimulated on antibody-coated dishes.

[c] Data from TIRF images using Jurkat cells co-expressing DLC-mEGFP and S312A mutant CLIP-170-TagRFP-T stimulated on antibody-coated dishes.

[d] Data from TIRF images using Jurkat cells co-expressing dynactin-mEGFP and wild-type CLIP-170-TagRFP-T stimulated on antibody-coated dishes.

[e] Average of [+] [e] is the average of the [+] velocities of the followings (indicated by superscript e): WT CLIP-170 not colocalised, stimulated; WT CLIP-170 not colocalised, unstimulated; dynactin not colocalised, stimulated; CLIP-170 & dynactin colocalised, stimulated.

[f] Average of [+] [f] is the average of the [+] velocities of the followings (indicated by superscript f): WT CLIP-170 & DLC colocalised, stimulated; WT CLIP-170 & DLC colocalised, unstimulated.

Table 3.4 Movement durations of dynein clusters (source data for Fig. 3.4A,B & 3.5A-C)

	Movement duration of dynein clusters (s)			
	Minus-end movement [–] [a]	$N_{cluster}$	Plus-end tracking [+] [b]	$N_{cluster}$
Stimulated [c]	16.1 ± 8.4 [e]	43	8.9 ± 3.0 [f]	16
Unstimulated [c]	14.3 ± 7.5 [e]	13	8.3 ± 2.5 [f]	3
Stimulated (S312A) [d]	18.5 ±14.6 [e]	38	ND	–
Average	16.8 ± 11.2 [g]	94	8.8 ± 2.9	19

Data are mean ± SD. $N_{cluster}$ indicates the number of clusters.

[a] All of the minus-end-directed clusters of dynein were not colocalised with CLIP-170 clusters.

[b] All of the plus-end tracking clusters of dynein were colocalised with CLIP-170 clusters.

[c] Data from TIRF images using Jurkat cells co-expressing DLC-mEGFP and wild-type CLIP-170-TagRFP-T stimulated and unstimulated on antibody-coated dishes.

[d] Data from TIRF images using Jurkat cells co-expressing DLC-mEGFP and S312A mutant CLIP-170-TagRFP-T stimulated on antibody-coated dishes.

[e] No significant difference among these three assessed using *t*-tests.

[f] No significant difference between these two assessed using *t*-tests.

[g] This value is an underestimation due to photobleaching.

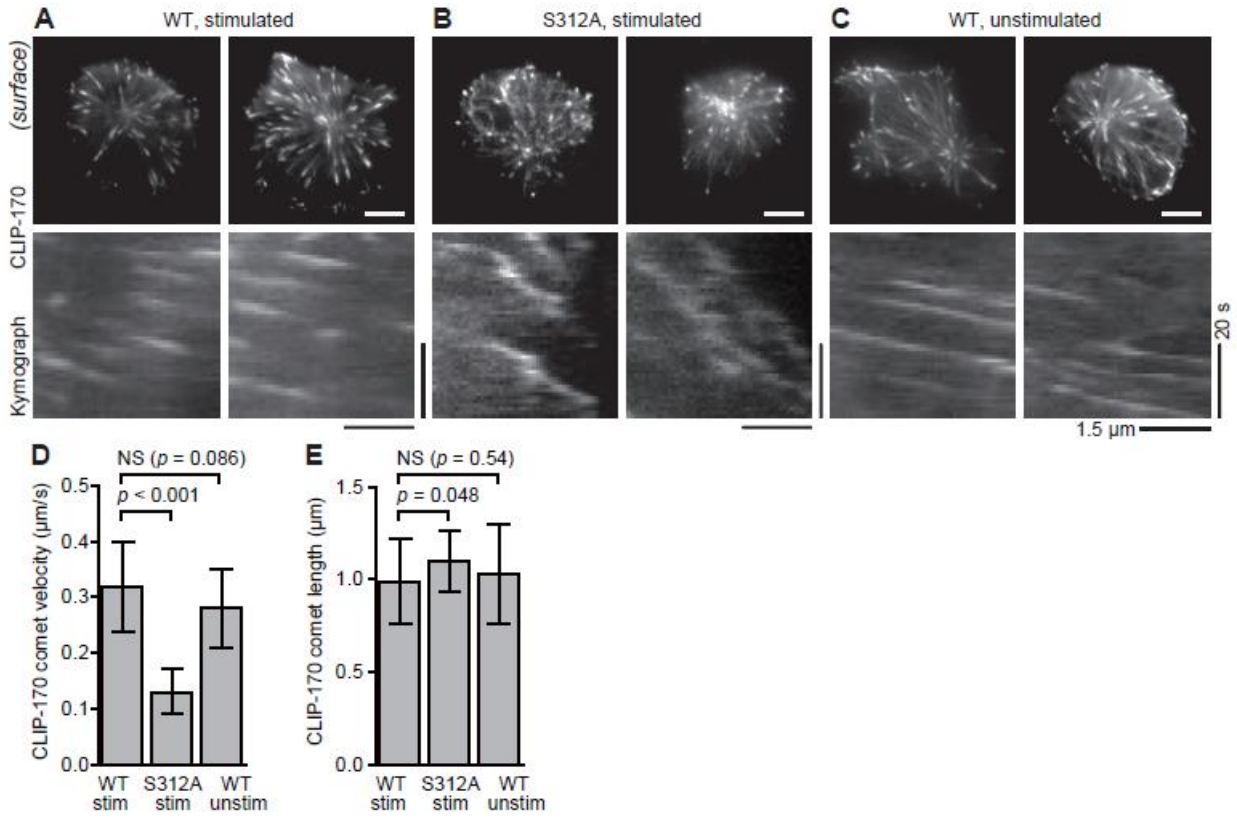

Figure 3.1 CLIP-170 phosphorylation up-regulates microtubule plus-end dynamics, but T cell stimulation does not. (**A-C**) TIRF live-cell images (top) and kymographs (bottom) of CLIP-170 comets and microtubule plus-end dynamics visualised using C-terminal mEGFP-tagged CLIP-170s: wild-type in stimulated cells (**A**), S312A mutant in stimulated cells (**B**), and wild-type in unstimulated cells (**C**) (see Movie S1). (**D**,**E**) The velocity (**D**) and the length (**E**) of CLIP-170 comets, quantified using the images. Bars in TIRF images, 5 µm; horizontal and vertical bars in kymographs, 1.5 µm and 20 s, respectively. Data are means ± SD. Source data, Table 3.2.

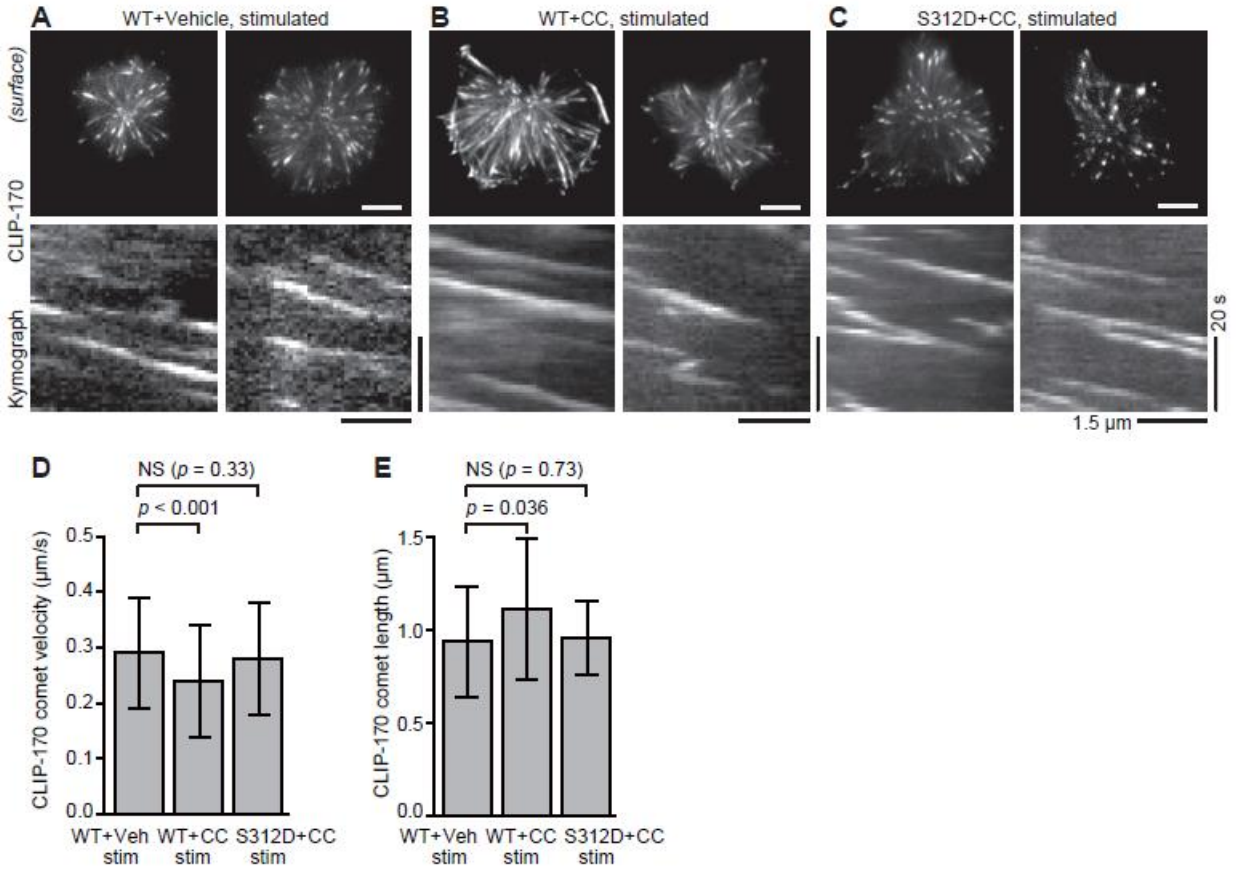

Figure 3.2 CLIP-170 phosphorylation at Ser-312 by AMPK up-regulates the microtubule plus-end dynamics. (**A-C**) TIRF live-cell images (top) and kymograph (bottom) of CLIP-170 comets and microtubule plus-end dynamics visualized using mEGFP-tagged CLIP-170s: wild-type in the presence of vehicle alone (0.2% DMSO, A) or 20 µM compound C (AMPK inhibitor, **B**), and phosphomimetic S312D mutant in the presence of 20 µM compound C (**C**). (**D**,**E**) The velocity (**D**) and the length (**E**) of CLIP-170 comets quantified using fluorescence images. Jurkat cells were stimulated with the anti-CD3ε/anti-CD28 antibodies coated on glass bottom dishes. Scale bar in TIRF images, 5 µm; horizontal and vertical scale bars in kymographs, 1.5 µm and 20 s, respectively. Data are means ± SD. Source data, Table 3.2.

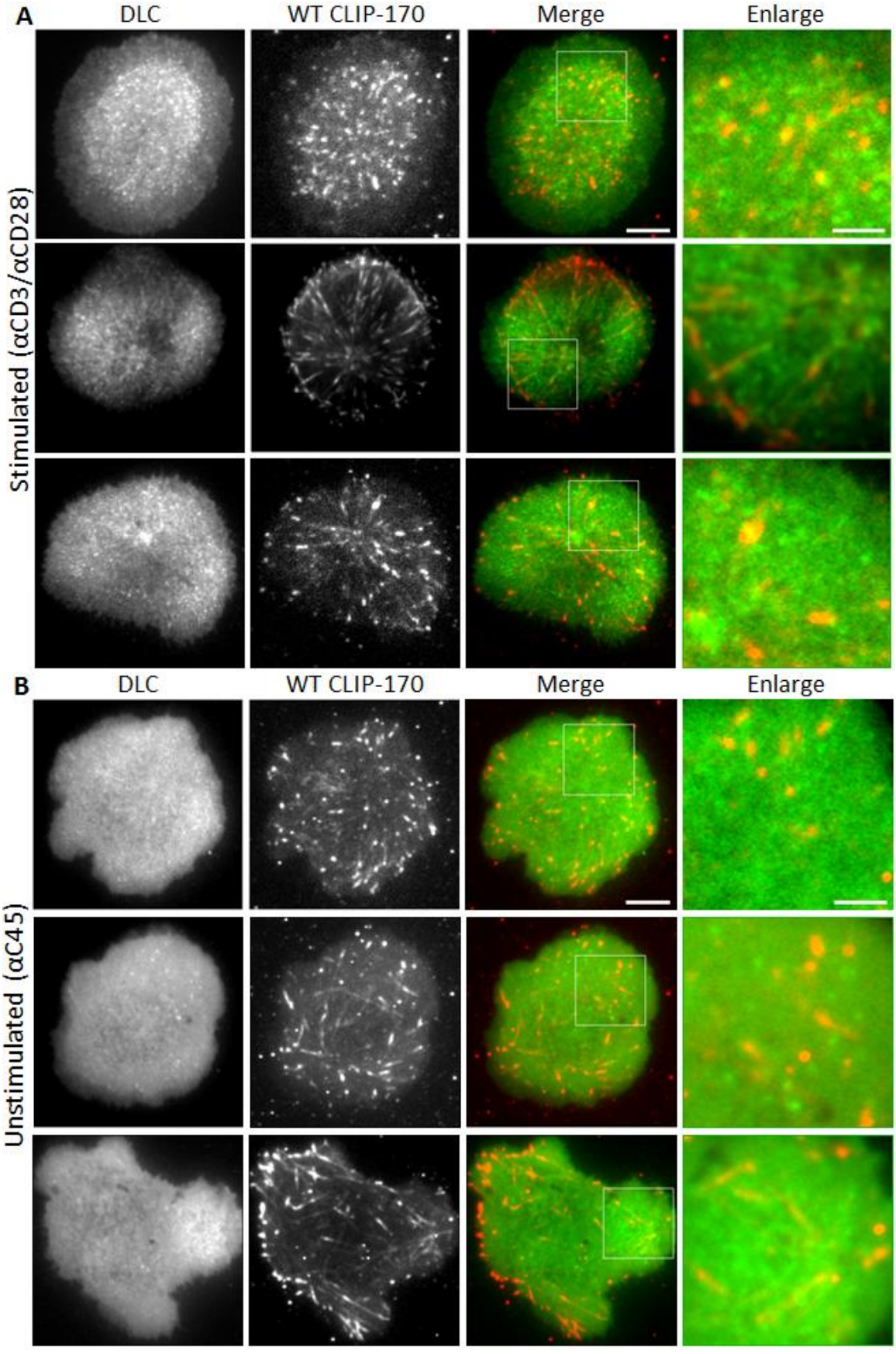
A
DLC
WT CLIP-170
Merge
Enlarge
Stimulated (αCD3/αCD28)
B
DLC
WT CLIP-170
Merge
Enlarge
Unstimulated (αC45)

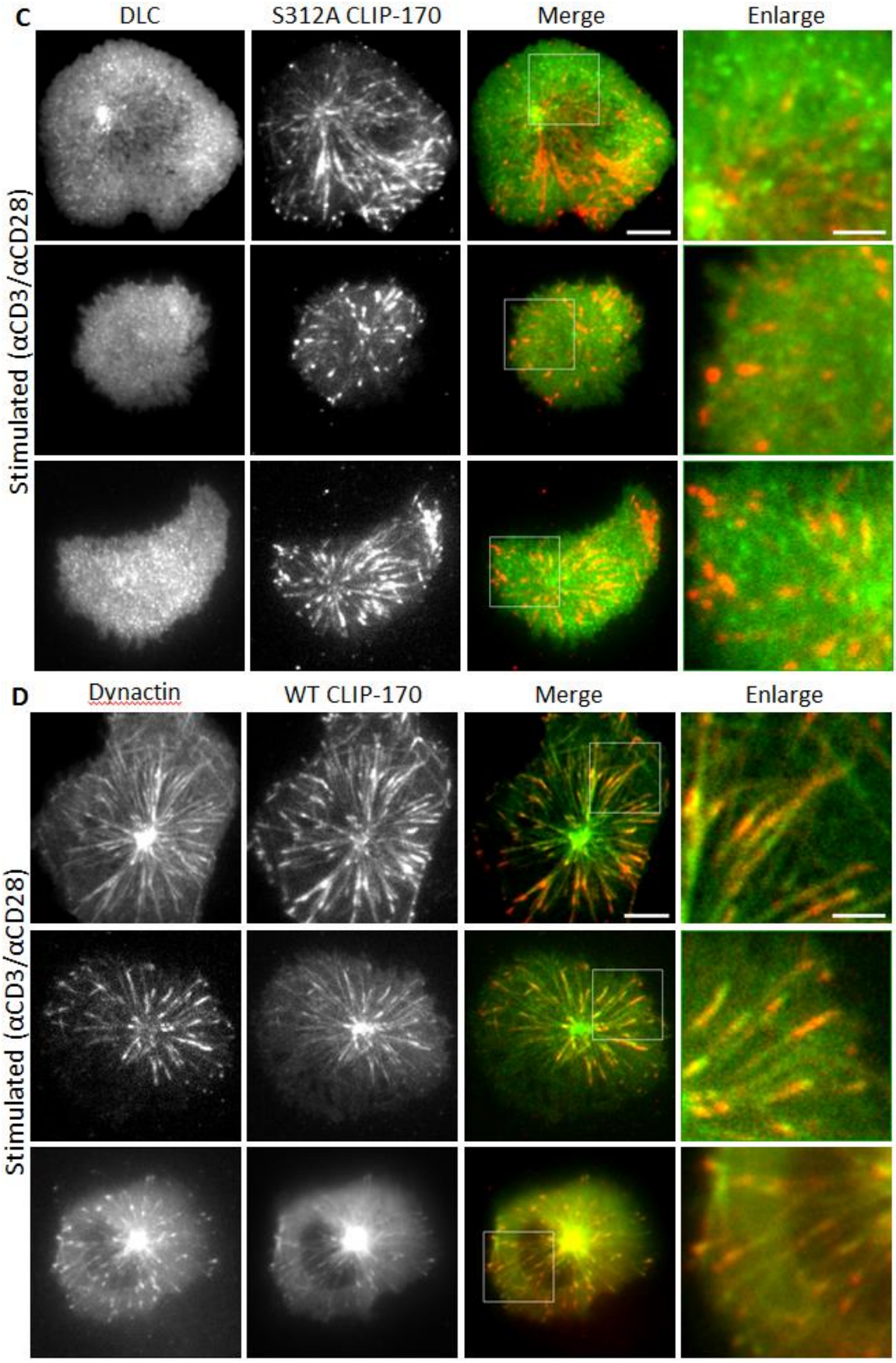
C
DLC
S312A CLIP-170
Merge
Enlarge
Stimulated (αCD3/αCD28)
D
Dynactin
WT CLIP-170
Merge
Enlarge
Stimulated (αCD3/αCD28)

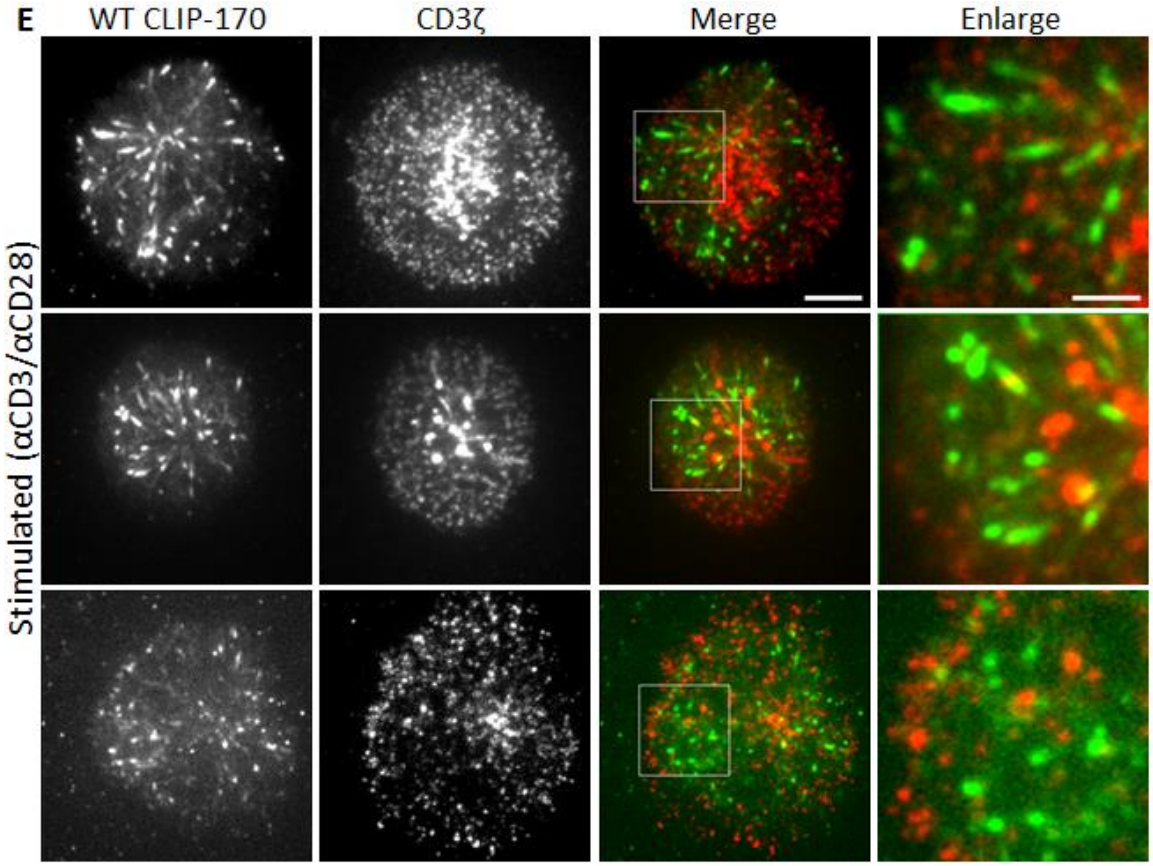
E
WT CLIP-170
CD3ζ
Merge
Enlarge
Stimulated (αCD3/αCD28)

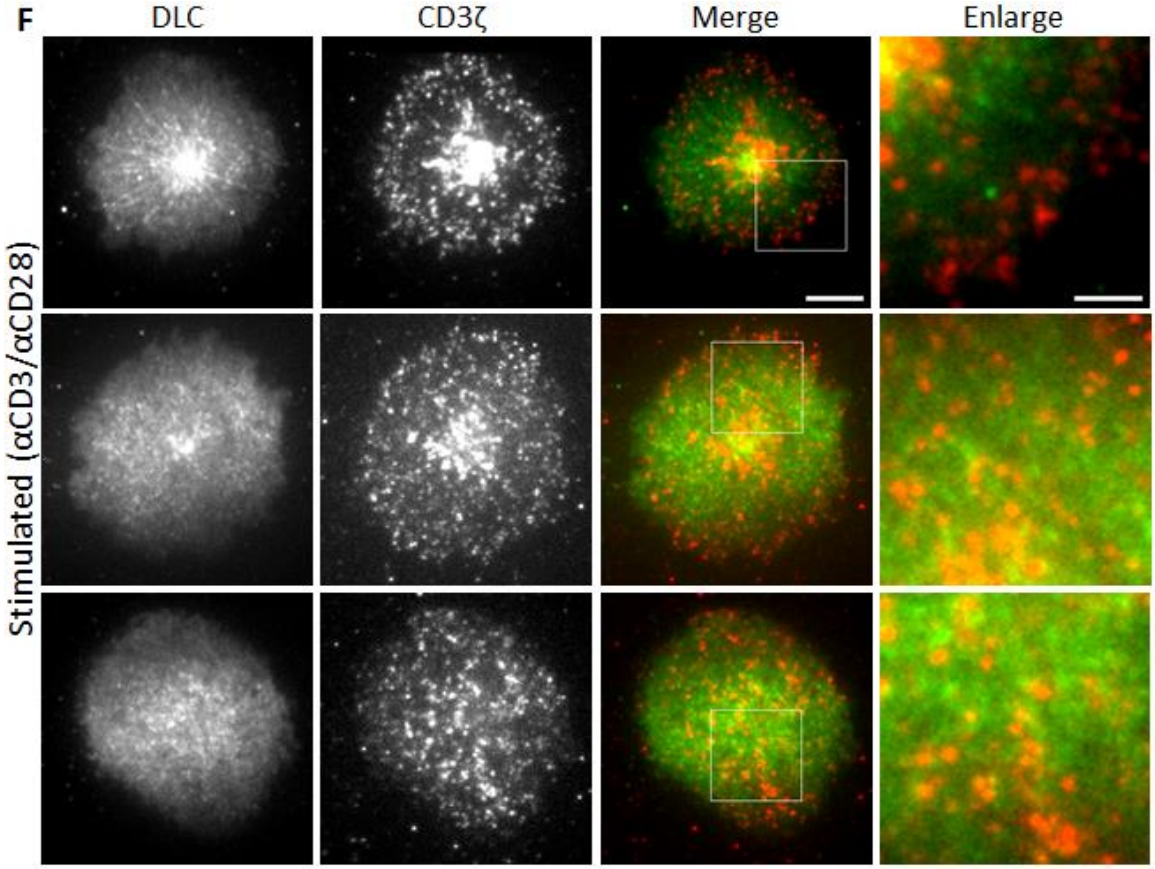
F
DLC
CD3ζ
Merge
Enlarge
Stimulated (αCD3/αCD28)

Figure 3.3 Simultaneous dual-colour TIRF live-cell imaging showing the localisations of the clusters of CLIP-170, dynein, dynactin and the TCR/CD3 complex. Jurkat cells expressing dynein light chain (DLC)-mEGFP (left; green in merged images) and wild-type CLIP-170-TagRFP-T (2nd left; red in merged images) (**A**,**B**), DLC-mEGFP (left; green) and S312A mutant CLIP-170-TagRFP-T (2nd left; red) (**C**), dynactin-mEGFP (left; green) and CLIP-170-TagRFP-T (2nd left; red) (**D**), CLIP-170-mEGFP (left; green) and CD3ζ-TagRFP-T (2nd left; red) (**E**), DLC-mEGFP (left; green) and CD3ζ-TagRFP-T (2nd left; red) (**F**) were stimulated with the anti-CD3ε/anti-CD28 antibodies (**A**, **C**-**F**) or unstimulated with the control anti-CD45 antibody (**B**) coated on glass bottom dishes. The boxed regions in the merged images are enlarged (right). Bars for images (left, 2nd left, merged) and enlarged images are 5 μm and 2 μm, respectively.

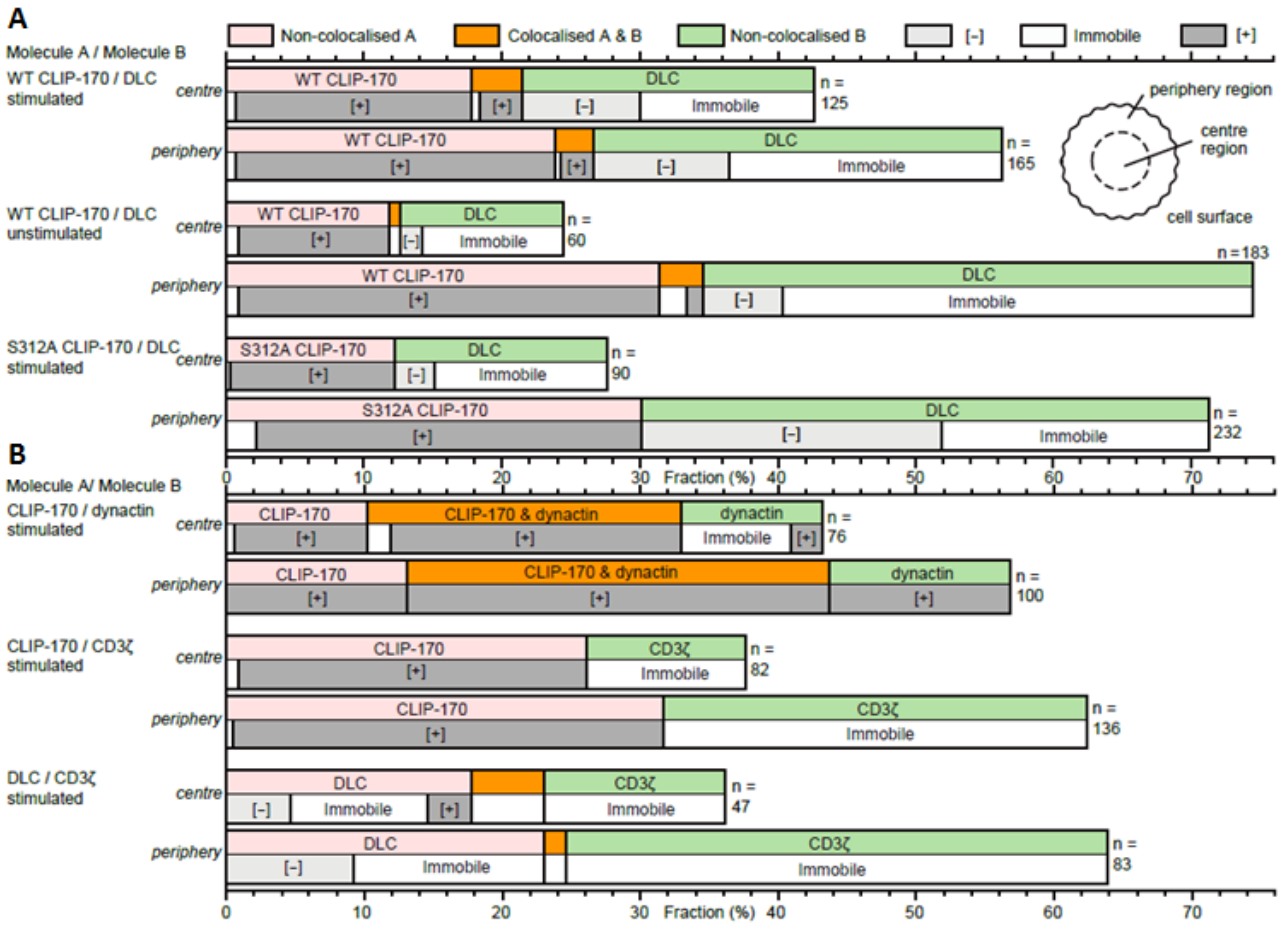

Figure 3.4 Coexistence of plus-end- and minus-end-directed dynein at the centre, and increased dynein relocation to the centre requires both stimulation and CLIP-170 phosphorylation. (**A**) Fractions of colocalisation between clusters of the two molecules (upper) at the centre or periphery region analysed using the images in Fig. 3.3 panels A-C. Note that the total of all the fractions at the centre and periphery is 100%. The fractions are further classified by translocation (lower): plus-end- or minus-end-directed, or immobile. (**B**) Colocalisation and translocation of CLIP-170 and dynactin, CLIP-170 and the TCR/CD3 complex, and dynein and the TCR/CD3 complex are shown as the same as in panel A analysed using the images in Fig. 3.3 panels D-F.

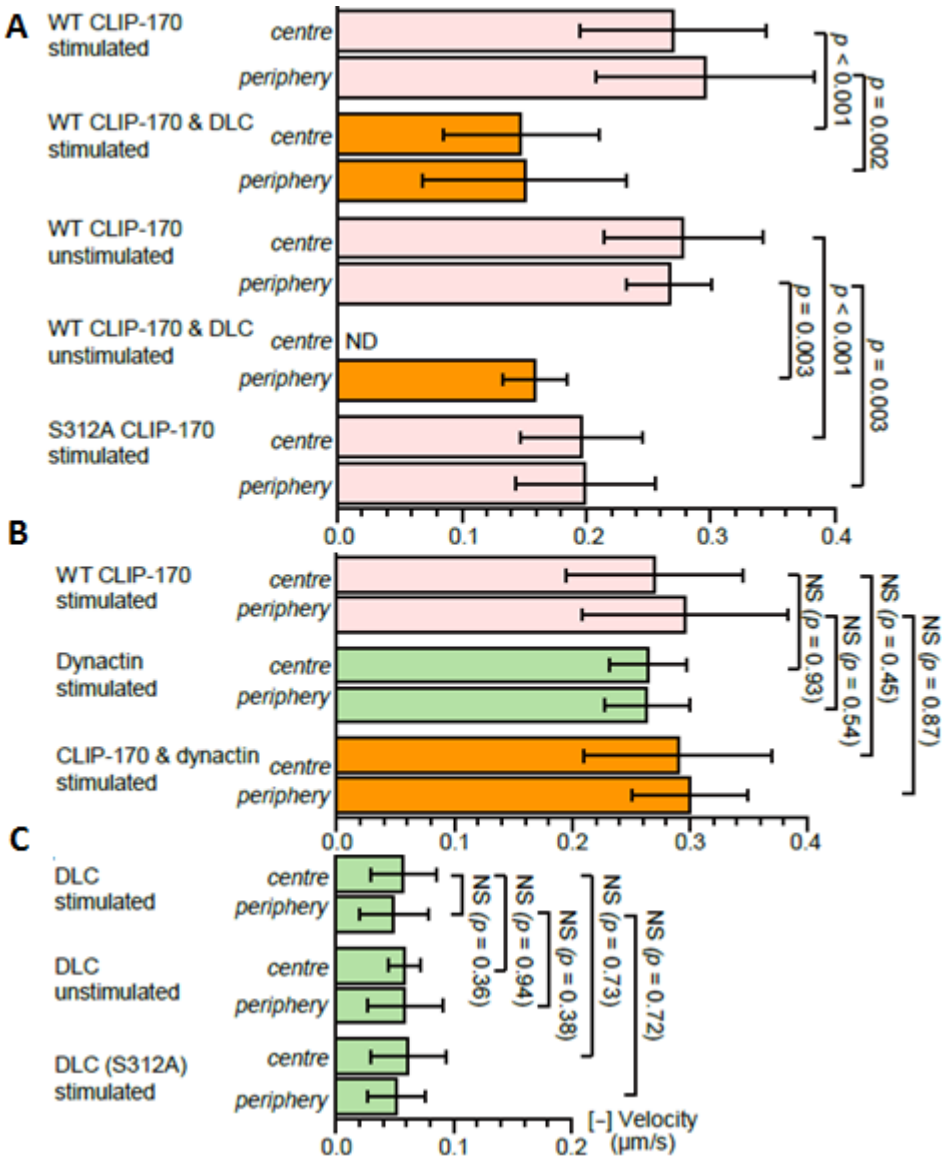

Figure 3.5 The velocities of plus-end tracking clusters of CLIP-170, dynactin and dynein light chain (DLC). (**A**,**B**) The velocities of plus-end tracking of the clusters quantified using the images in Figure 3.3 panels A-C and D-F corresponding to panels Figure 3.4 panel A and B, respectively. The velocities of wild-type CLIP-170 were re-plotted in panel B from panel A for comparison. See Table 3.3 for details. (**C**) The velocities of minus-end-directed movement of non-colocalised dynein clusters, quantified using the images in Fig. 3.3 panel A-C corresponding to Fig. 3.4 panel A. DLC (S312A), using the images of pair S312/DLC. Data are means ± SD. Source data for panels A-C, Table 3.3.

3.4 Discussion

In contrast to the importance of MTOC repositioning during T cell activation, the molecular mechanisms underlying this process remain unknown. In this study, a novel role of CLIP-170 in regulating dynein localization analysed by simultaneous dual-colour fluorescence live-cell microscopy was reported. Phosphorylated CLIP-170 is essential for dynein recruitment to the plus-end tracking. T cell stimulation increases dynein in minus-end-directed movement. Both plus-end- and minus-end-directed translocation of dynein are necessary for dynein relocation to the immunological synapse. Based on these results, we propose a model of MTOC repositioning (Fig. 3.6).

There are several discussions concerning the motive force involved for MTOC repositioning:

(1) a dynein-driven pulling mechanism, where dynein is anchored at the immunological synapse and its processive activity pulls on the microtubules

(2) a capture-shrinkage mechanism, where cortically bound dynein interacts with the plus end of a microtubule in a way as to couple the subsequent microtubule depolymerisation[13]

(3) a dynein-independent mechanism, an actin-dependent model, where microtubules are anchored to the peripheral F-actin ring and forces are exerted on microtubules by expansion of the F-actin ring, together with forces generated by cortex-associated dynein[12]

The findings consolidated in this study support the dynein-driven pulling mechanism.

The rate of MTOC repositioning was reported to be 0.054 ± 0.013 µm/s (3.26 ± 0.77 µm/min)[9]. The present result of the average velocity 0.054 ± 0.028 µm/s of minus-end-directed dynein is in good accordance with the MTOC repositioning rate. Recently, a structural study using cryo-electron microscopy on the activation mechanism of cytoplasmic dynein revealed that dynein, which does not form a complex with dynactin and cargo activator protein, remains in a “weakly

processive" state[23]. A study using single-molecule assays reported that the *in vitro* velocity of dynein alone is 0.079 ± 0.011 μm/s[20], which also corresponds well with the present result. These multiple lines of findings support the dynein-driven pulling mechanism, and indicate that MTOCs undergoing repositioning during T cell activation is pulled by immobilised cytoplasmic dynein in the "weakly processive" state at the immunological synapse (Fig. 3.6, "pull").

Previously, the role of CLIP-170 on MTOC repositioning during T cell activation has not been elucidated. Dissection of MTOC repositioning into the two directions has shed a new light on it. The imaging studies using CLIP-170 phosphosite mutants reveal that MTOC parallel transposition, centreing, requires both CLIP-170 phosphorylation and T cell stimulation, whereas MTOC perpendicular transposition is caused solely by stimulation without requiring CLIP-170 phosphorylation. In addition to this asymmetric joint role of CLIP-170 phosphorylation and T cell stimulation, we found one more difference in their role: CLIP-170 phosphorylation up-regulates microtubule plus-end dynamics, whereas T cell stimulation does not affect plus-end dynamics. These seemingly contradictory findings have been solved by the simultaneous dual-colour fluorescence live-cell microscopy as follows: colocalisation of dynein with CLIP-170 is caused solely by CLIP-170 phosphorylation, and is increased by T cell stimulation. Plus-end-directed dynein is only observed in colocalised dynein with CLIP-170. Thus, CLIP-170 phosphorylation regulates MTOC repositioning via dynein recruitment but not via microtubule plus-end dynamics.

The simultaneous dual-colour fluorescence imaging and mobility analysis enabled us to study characteristics of interactions and dynamics of CLIP-170, dynein, dynactin and the TCR/CD3 complex. CLIP-170 alone or together with dynactin translocates to the plus-end at 0.28 ± 0.07 μm/s. This corresponds well with the rate of microtubule growth (0.30 ± 0.13 μm/s in LLCPK1 cells)[42]. Meanwhile, the plus-end-directed velocity of colocalised CLIP-170 and dynein is slower than that of non-colocalised CLIP-170, indicating that colocalisation of dynein with CLIP-170 acts as a source of resistance to the plus-end tracking. Additionally, the lifetime of the plus-end-directed dynein cluster colocalised with

CLIP-170 is almost half of that of the minus-end-directed dynein cluster. These observations may also suggest that the colocalised dynein interacts with other proteins, such as anchor proteins immobilised to the cell membrane (Fig. 3.6, “recruit” and “release”).

Recently, the balance between the microtubule plus-end tracking and minus-end-directed motility of cytoplasmic dynein is receiving attention[16]. Here we have found that their coexistence is indispensable for MTOC repositioning. Among the present findings, both CLIP-170 phosphorylation and T cell stimulation are required for:

(1) plus-end-directed dynein, which is only observed in colocalised dynein with CLIP-170 (Fig. 3.6, “recruit”)

(2) coexistence of plus-end- and minus-end-directed dynein at the centre region

(3) dynein relocation to the centre (Fig. 3.6, “mobilise” and “anchor”)

(4) MTOC repositioning and full activation of T cells

These findings indicate that coexistence of plus-end- and minus-end-directed dynein is a key determinant of dynein relocation and MTOC repositioning.

This key determinant is generated by recruiting dynein to the complex with phosphorylated CLIP-170, and is increased by T cell stimulation (especially at the centre, largely increased). This finding raises a question how dynein is recruited to plus-end tracking by phosphorylated CLIP-170. The recruitment could be due to phosphorylation of dynein caused by weakening of the anchoring to the cell surface of contact, since phosphorylation of dynein intermediate chain has been reported to reduce its interaction with NDEL1[43], the homologue of NDE1, the anchor candidate[24,25], with a high sequence similarity. Meanwhile, NDE1 and dynactin forms mutually exclusive complexes with the dynein intermediate chain[25]. Furthermore, two isoforms DCTN1A and DCTN1B of dynactin 1, the largest subunit of dynactin, have antagonistic functions on dynein activity: the tripartite complex of dynein-dynactin-cargo adaptor BICD2 containing DCTN1A exhibits highly processive movement; the complex of dynein-dynactin containing

DCTN1B shows no apparent processive movement[21]. These findings suggest that the dynactin containing DCTN1B could function as a recruiter of dynein. The molecular mechanisms underlying the recruitment of dynein to plus-end tracking and the anchoring of dynein remain to be solved.

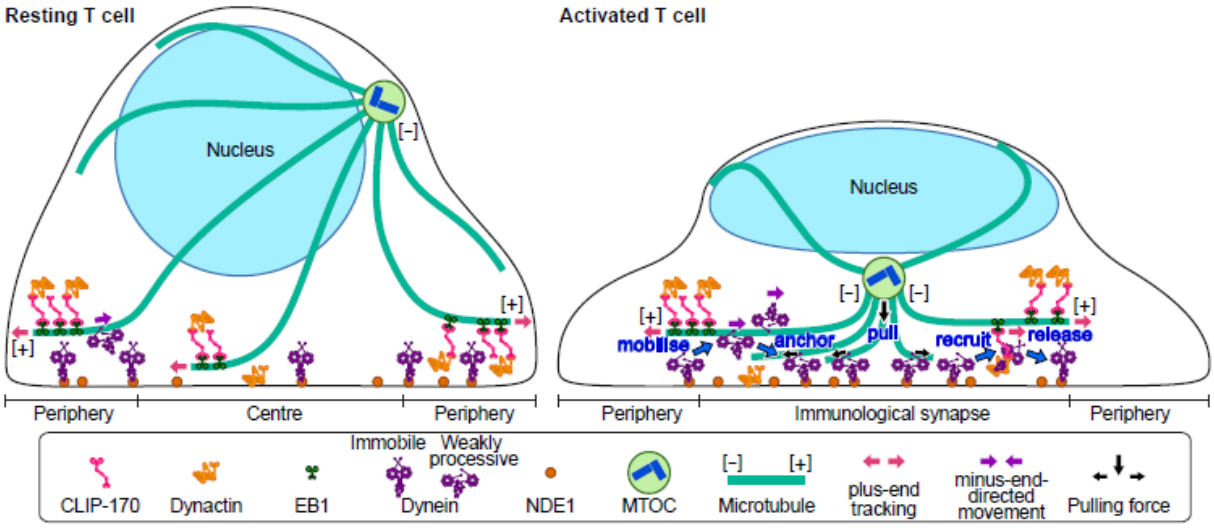

Figure 3.6 A schematic model for a key role of CLIP-170 in MTOC repositioning during T cell activation by regulating cytoplasmic dynein relocation to the immunological synapse. In resting Jurkat T cells, the majority of dynein is immobile on the contacted cell surface, and is located at the periphery region. T cell stimulation increases the fraction of dynein undergoing minus-end-directed motility ("mobilise"), which is a "weakly processive" state, i.e. not the highly processive complex with cargo and dynactin. Then, the dynein anchored to the surface after translocation less than one or two micrometres ("anchor"). Alongside this, stimulation induces some fraction of dynein to colocalise with CLIP-170 and dynactin, and follow the plus-end tracking ("recruit"). The recruited dynein has slower velocity and shorter lifetime, suggesting its interaction with membrane proteins, probably anchor proteins. After tracking of one or two micrometres, the dynein is released from the complex and anchored ("release"). As a result of coexistence of plus-end- and minus-end-directed translocation, dynein relocation increases to the centre region of the contact surface, the immunological synapse, where "anchored" dynein molecules are immobile and or weakly processive at a velocity in good agreement with the velocity of MTOC repositioning. "Anchored" and weakly processive dynein pulls the microtubules and the MTOC ("pull"), which causes MTOC repositioning near the immunological synapse and full activation of T cells. Phosphorylation of CLIP-170 is essential for dynein recruitment to the plus-end tracking and for dynein relocation.

Chapter 4

Conclusion

This work demonstrates a novel and indispensable role of CLIP-170 in MTOC repositioning and full activation of T cells. Coexistence of plus-end- and minus-end-directed dynein is generated via the joint role of CLIP-170 phosphorylation and T cell stimulation. This is essential for dynein relocation to the immunological synapse, where the immobilised dynein may pull the MTOC.

These present findings may be helpful towards the understanding of tumour immunotherapy, which involved cytotoxic T lymphocyte antigen 4 (CTLA-4) as the therapeutic target. Previous study has reported the polarization of CTLA-4 toward the TCR engagement site is likely related to the rapid repositioning of MTOC to the APC in T cell. Because CTLA-4 is a negative regulator for T cell activation, these seemingly contradicting findings concerning the importance of MTOC repositioning in T cell activation may be a new ground to explore.

Besides, this work may also shed new light on biological processes involving microtubule binding proteins and microtubule dynamics. It will be interesting to observe the interplay of CLIP-170 and other microtubule-binding proteins in the bipolar spindle assembly during cell division, which is still poorly understood in the field of oncology.

References

1. Grakoui, A. *et al.* The Immunological Synapse: A Molecular Machine Controlling T Cell Activation. *Science* **285,** 221–227 (1999).
2. Monks, C. R. F., Freiberg, B. A., Kupfer, H., Sciaky, N. & Kupfer, A. Three-dimensional segregation of supramolecular activation clusters in T cells. *Nature* **395,** 82–86 (1998).
3. Yokosuka, T. *et al.* Newly generated T cell receptor microclusters initiate and sustain T cell activation by recruitment of Zap70 and SLP-76. *Nat. Immunol.* **6,** 1253–1262 (2005).
4. Geiger, B., Rosen, D. & Berke, G. Spatial relationships of microtubule-organizing centers and the contact area of cytotoxic T lymphocytes and target cells. *J. Cell Biol.* **95,** 137–143 (1982).
5. Kuhn, J. R. & Poenie, M. Dynamic Polarization of the Microtubule Cytoskeleton during CTL-Mediated Killing. *Immunity* **16,** 111–121 (2002).
6. Combs, J. *et al.* Recruitment of dynein to the Jurkat immunological synapse. *Proc. Natl. Acad. Sci. U. S. A.* **103,** 14883–14888 (2006).
7. Martín-Cófreces, N. B. *et al.* MTOC translocation modulates IS formation and controls sustained T cell signaling. *J. Cell Biol.* **182,** 951–962 (2008).
8. Quann, E. J., Merino, E., Furuta, T. & Huse, M. Localized diacylglycerol drives the polarization of the microtubule-organizing center in T cells. *Nat. Immunol.* **10,** 627–635 (2009).
9. Yi, J. *et al.* Centrosome repositioning in T cells is biphasic and driven by microtubule end-on capture-shrinkage. *J. Cell Biol.* **202,** 779–792 (2013).
10. Kupfer, A., Dennert, G. & Singer, S. J. Polarization of the Golgi apparatus and the microtubule-organizing center within cloned natural killer cells bound to their targets. *Proc. Natl. Acad. Sci. U. S. A.* **80,** 7224–7228 (1983).
11. Stinchcombe, J. C., Majorovits, E., Bossi, G., Fuller, S. & Griffiths, G. M. Centrosome polarization delivers secretory granules to the immunological synapse. *Nature* **443,** 462–465 (2006).
12. Wang, J. C. *et al.* The Rap1–cofilin-1 pathway coordinates actin reorganization and MTOC polarization at the B cell immune synapse. *J Cell Sci* **130,** 1094–1109 (2017).
13. Laan, L. *et al.* Cortical dynein controls microtubule dynamics to generate pulling

forces that position microtubule asters. *Cell* **148,** 502–514 (2012).

14. Vallee, R. B., McKenney, R. J. & Ori-McKenney, K. M. Multiple modes of cytoplasmic dynein regulation. *Nat. Cell Biol.* **14,** 224–230 (2012).
15. Cianfrocco, M. A., DeSantis, M. E., Leschziner, A. E. & Reck-Peterson, S. L. Mechanism and regulation of cytoplasmic dynein. *Annu. Rev. Cell Dev. Biol.* **31,** 83–108 (2015).
16. Jha, R., Roostalu, J., Cade, N. I., Trokter, M. & Surrey, T. Combinatorial regulation of the balance between dynein microtubule end accumulation and initiation of directed motility. *EMBO J.* **36,** 3387–3404 (2017).
17. McKenney, R. J., Huynh, W., Tanenbaum, M. E., Bhabha, G. & Vale, R. D. Activation of cytoplasmic dynein motility by dynactin-cargo adapter complexes. *Science* **345,** 337–341 (2014).
18. Schlager, M. A., Hoang, H. T., Urnavicius, L., Bullock, S. L. & Carter, A. P. In vitro reconstitution of a highly processive recombinant human dynein complex. *EMBO J.* **33,** 1855–1868 (2014).
19. Torisawa, T. *et al.* Autoinhibition and cooperative activation mechanisms of cytoplasmic dynein. *Nat. Cell Biol.* **16,** 1118–1124 (2014).
20. Belyy, V. *et al.* The mammalian dynein-dynactin complex is a strong opponent to kinesin in a tug-of-war competition. *Nat. Cell Biol.* **18,** 1018–1024 (2016).
21. Kobayashi, T., Miyashita, T., Murayama, T. & Toyoshima, Y. Y. Dynactin has two antagonistic regulatory domains and exerts opposing effects on dynein motility. *PLOS ONE* **12,** e0183672 (2017).
22. Schroeder, C. M. & Vale, R. D. Assembly and activation of dynein-dynactin by the cargo adaptor protein Hook3. *J. Cell Biol.* **214,** 309–318 (2016).
23. Zhang, K. *et al.* Cryo-EM Reveals How Human Cytoplasmic Dynein Is Auto-inhibited and Activated. *Cell* **169,** 1303-1314.e18 (2017).
24. Lam, C., Vergnolle, M. A. S., Thorpe, L., Woodman, P. G. & Allan, V. J. Functional interplay between LIS1, NDE1 and NDEL1 in dynein-dependent organelle positioning. *J. Cell Sci.* **123,** 202–212 (2010).
25. Nath, S. *et al.* Dynein Separately Partners with NDE1 and Dynactin To Orchestrate T Cell Focused Secretion. *J. Immunol. Baltim. Md 1950* **197,** 2090–2101 (2016).
26. Wu, X., Xiang, X. & Hammer, J. A. Motor proteins at the microtubule plus-end.

Trends Cell Biol. **16,** 135–143 (2006).

27. Watson, P. & Stephens, D. J. Microtubule plus-end loading of p150(Glued) is mediated by EB1 and CLIP-170 but is not required for intracellular membrane traffic in mammalian cells. *J. Cell Sci.* **119,** 2758–2767 (2006).
28. Dixit, R. *et al.* Microtubule plus-end tracking by CLIP-170 requires EB1. *Proc. Natl. Acad. Sci. U. S. A.* **106,** 492–497 (2009).
29. Bieling, P. *et al.* Reconstitution of a microtubule plus-end tracking system in vitro. *Nature* **450,** 1100–1105 (2007).
30. Roberts, A. J., Goodman, B. S. & Reck-Peterson, S. L. Reconstitution of dynein transport to the microtubule plus end by kinesin. *eLife* **3,** e02641 (2014).
31. Rickard, J. E. & Kreis, T. E. Identification of a novel nucleotide-sensitive microtubule-binding protein in HeLa cells. *J. Cell Biol.* **110,** 1623–1633 (1990).
32. Scheel, J. *et al.* Purification and analysis of authentic CLIP-170 and recombinant fragments. *J. Biol. Chem.* **274,** 25883–25891 (1999).
33. Bieling, P. *et al.* CLIP-170 tracks growing microtubule ends by dynamically recognizing composite EB1/tubulin-binding sites. *J. Cell Biol.* **183,** 1223–1233 (2008).
34. Slep, K. C. Structural and mechanistic insights into microtubule end-binding proteins. *Curr. Opin. Cell Biol.* **22,** 88–95 (2010).
35. Lansbergen, G. *et al.* Conformational changes in CLIP-170 regulate its binding to microtubules and dynactin localization. *J. Cell Biol.* **166,** 1003–1014 (2004).
36. Nakano, A. *et al.* AMPK controls the speed of microtubule polymerization and directional cell migration through CLIP-170 phosphorylation. *Nat. Cell Biol.* **12,** 583–590 (2010).
37. Tokunaga, M., Kitamura, K., Saito, K., Iwane, A. H. & Yanagida, T. Single molecule imaging of fluorophores and enzymatic reactions achieved by objective-type total internal reflection fluorescence microscopy. *Biochem. Biophys. Res. Commun.* **235,** 47–53 (1997).
38. Tokunaga, M., Imamoto, N. & Sakata-Sogawa, K. Highly inclined thin illumination enables clear single-molecule imaging in cells. *Nat. Methods* **5,** 159–161 (2008).
39. Kim, J.-E. & White, F. M. Quantitative analysis of phosphotyrosine signaling networks triggered by CD3 and CD28 costimulation in Jurkat cells. *J. Immunol. Baltim. Md 1950* **176,** 2833–2843 (2006).

40. Jhun, B. S. *et al.* Inhibition of AMP-activated protein kinase suppresses IL-2 expression through down-regulation of NF-AT and AP-1 activation in Jurkat T cells. *Biochem. Biophys. Res. Commun.* **351,** 986–992 (2006).
41. Zhou, G. *et al.* Role of AMP-activated protein kinase in mechanism of metformin action. *J. Clin. Invest.* **108,** 1167–1174 (2001).
42. Salaycik, K. J., Fagerstrom, C. J., Murthy, K., Tulu, U. S. & Wadsworth, P. Quantification of microtubule nucleation, growth and dynamics in wound-edge cells. *J. Cell Sci.* **118,** 4113–4122 (2005).
43. Gao, F. J. *et al.* GSK-3ß Phosphorylation of Cytoplasmic Dynein Reduces Ndel1 Binding to Intermediate Chains and Alters Dynein Motility. *Traffic* **16,** 941–961 (2015).
44. Zacharias, D. A., Violin, J. D., Newton, A. C. & Tsien, R. Y. Partitioning of lipid-modified monomeric GFPs into membrane microdomains of live cells. *Science* **296,** 913–916 (2002).
45. Trinh, R., Gurbaxani, B., Morrison, S. L. & Seyfzadeh, M. Optimization of codon pair use within the (GGGGS)3 linker sequence results in enhanced protein expression. *Mol. Immunol.* **40,** 717–722 (2004).
46. Shimozono, S. & Miyawaki, A. Engineering FRET constructs using CFP and YFP. *Methods Cell Biol.* **85,** 381–393 (2008).
47. Ito, Y., Sakata-Sogawa, K. & Tokunaga, M. A facile preparation of glass-supported lipid bilayers for analyzing molecular dynamics. *Anal. Sci. Int. J. Jpn. Soc. Anal. Chem.* **30,** 1103–1106 (2014).
48. Shaner, N. C. *et al.* Improving the photostability of bright monomeric orange and red fluorescent proteins. *Nat. Methods* **5,** 545–551 (2008).
49. Bustin, S. A. *et al.* The MIQE guidelines: minimum information for publication of quantitative real-time PCR experiments. *Clin. Chem.* **55,** 611–622 (2009).
50. Schürmann, M., Scholze, J., Müller, P., Guck, J. & Chan, C. J. Cell nuclei have lower refractive index and mass density than cytoplasm. *J. Biophotonics* **9,** 1068–1076 (2016).
51. Schneider, C. A., Rasband, W. S. & Eliceiri, K. W. NIH Image to ImageJ: 25 years of image analysis. *Nat. Methods* **9,** 671–675 (2012).

Acknowledgements

The completion of this work is the results of combined contribution of all the following outstanding individuals and institutions:

Professor Makio TOKUNAGA, my academic supervisor. I thank him for accepting me into his remarkable laboratory, for his countless constructive advice toward my experimental findings and I am humbled to be given this opportunity to learn his traits. I am indebted to Tokunaga-sensei for all the academic and non-academic guidance he has given me throughout the period of my studies. My sincere gratitude towards his cares for me when I am in a foreign land on my own.

Associate Professor Kumiko SAKATA-SOGAWA, my former academic supervisor who had retired in March 2017. I thank her for the coaching given towards my experimental progress before and after the period of her retirement. For all the experimental techniques she had taught me and the academic guidance granted to me, I am immensely grateful.

Assistant Professor Yuma ITO, a senior and a friend. I thank him for keeping close attention towards my work and for teaching me all the fundamental experimental technique during my stay in the laboratory. I thank him for co-authoring our manuscript and it has been such a pleasure working with him throughout my stay in Japan. My sincere gratitude to him for uploading the microscopic images to me when I work on my thesis documentation in my hometown.

Dr. Yoko FUJII, the laboratory technician who has also retired in March 2017. I thank her for teaching me the technique for developing CLIP-170 clones, which were one of the main components for my PhD thesis script. Her tender cares towards the laboratory members were admirable and I am truly grateful to be part of the team.

Ms. Saori OYA, the laboratory administrative. My sincere gratitude for her contribution toward my stay in Japan, her warm assistance in helping me with the official documentation from academic paperwork to personal taxation, and I am deeply thankful to her genuine concern towards my well-being.

Mr. LIM Choon Hoo and **Ms. Cindy OOI Ah Leak**, my dad and mom. I thank them for their support and encouragement. I am sincerely indebted for their unconditional support, both morally and financially, without which, I would have never come this far on my own.

Mr. Kenkichi IWATA, the laboratory computer technician for maintaining my working desktop so that I could work on my experimental progress without hiccup.

Ms. Lim Chuey Szu, my sister. I thank her for lending me her company laptop to write my thesis when I am in need of a computer to prepare my thesis documentation and presentation slides.

The **Center for Biological Resources and Informatics** of Tokyo Tech, for assistance in sequence analysis.

The Academy of Computational Life Sciences (ACLS), for the abundance of opportunities granted and for funding my studies, without which, I would not have able to embark in this unique PhD journey.

All members of Professor Tokunaga's laboratory, I thank them for welcoming me and making my stay a pleasant adventure. Finally, I thank all who were involved in making this thesis possible.

Lim Wei Ming

Tokyo Institute of Technology

23th December 2018